Regional structural control on the Mont-Dore Plio-Quaternary volcanism (France)

Camille Daffos, Laurent Arbaret, Jean-Louis Bourdier, Charles Gumiaux

Journal of Volcanology and Geothermal Research 447 (2024) 108029

Contents lists available at ScienceDirect

Journal of Volcanology and Geothermal Research

journal homepage: www.journals.elsevier.com/journal-of-volcanology-and-geothermal-research

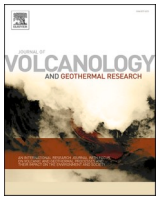

Regional structural control on the Mont-Dore Plio-Quaternary volcanism (France)

Camille Daffos, Laurent Arbaret *, Jean-Louis Bourdier, Charles Gumiaux

Université d'Orléans, CNRS/INSU, ISTO, UMR 7327, Orléans 45071, France

ARTICLE INFO

Keywords:
Polygenetic volcanism
Regional stress
Crustal faults
Fractures
Magma emplacement
Eruptive vent location

ABSTRACT

Magma transfer in the upper crust including emplacement at the surface of the Earth, have been regarded as largely controlled by the regional tectonic activity. While this relationship is well highlighted for systems like monogenetic, mostly basaltic, volcanic fields, the tectonic control on the transfer and emplacement of magmas in complex, polygenetic, volcanic systems, remains poorly documented in evolving tectonic settings. The Mont-Dore Plio-Quaternary volcanic complex (4.7 to 0.3 Ma) is one of such polygenetic volcanic fields as it is formed of three successive eruptive cycles: The caldera unit (3.3 to 2.2 Ma); The Aiguiller complex (2.5 to 1.5 Ma) and the Sancy stratovolcano unit (1.5 to 0.3 Ma).

Analyzing fractures, fault kinematics and regional lineaments in the Variscan basement, together with attitude of dikes and volcanic centers alignments of the three volcanic units, we document the influence of the brittle structuration of the underlying basement on the volcanism distribution over time while regional stress changed. The late-Variscan N02E0, and secondary N160, striking crustal faults were reactivated since the Oligocene and channeled at depth the magma, while similarly oriented faults and fractures triggered the final storage in the shallow crust and spatial distribution of the volcanic vents. This fault system continued to act from the Miocene to the present-day uplift, associated with new N020E striking, flat-lying, fractures. An exception arises during the upper Miocene while N060E and N135E striking faults enabled the development of the caldera unit in a NW-SE extensional context.

The emplacement of the three units from the mid-Pliocene to the end of the Pleistocene while a change in regional stress field conditions emerged at about 2.5 Ma exemplify the control of the brittle Variscan basement on the magmatic activity of the Mont-Dore Plio-Quaternary volcanic complex.

1. Introduction

At shallow depth, the magmatic plumbing system is mainly composed of magma-filled planar structures such as inclined sheets, horizontal sills that may aggregate to form laccoliths and magma chambers, and vertical dikes. Some of these can reach the surface, triggering volcanic events (Rubin, 1995; Gudmundsson, 2006; Tibaldi, 2015; Breitkreuz and Rocchi, 2018; Kavanagh, 2018; Gudmundsson, 2020). If magma transport is often regarded as largely controlled by the regional tectonic activity (Petford, 2000; Bursik, 2009; Cembrano and Lara, 2009 and references therein), the local stress field can be changed near crustal weak discontinuities, such as preexisting fractures, regional scale fault zones, and mechanically contrasted lithologies (Pollard, 1987; Gudmundsson, 2011; Menand, 2011; Maccaferri et al., 2011; Elshaafi and Gudmundsson, 2016; Kavanagh et al., 2018; Gudmundsson, 2020; Acocella, 2021). In addition, stress concentration nearby magma chambers at depth, and the load of composite volcanoes near the surface may interfere to modify the local stress field and thus control, together with the magmatic overpressure, the magma-filled sheets propagation or arrest (Gudmundsson and Brenner, 2005; Gudmundsson, 2006; Burchardt and Gudmundsson, 2009). In a pristine granitic basement, the stress field yields magma pathways by reactivating properly oriented preexisting fault and fracture networks or by creating new sets of fractures. If the regional tectonic exerts a control on magma ascent from the deep sources, it has also a significant role on magma differentiation and the associated volcanism activity by promoting, or not, the storage at shallow depth of large volumes of magmas (Cembrano and Moreno, 1994).

In intraplate volcanism, this relationship is well highlighted for monogenetic, mostly basaltic, volcanic fields (Connor, 1990; Connor

* Corresponding author.
E-mail address: Laurent.arbaret@univ-orleans.fr (L. Arbaret).

https://doi.org/10.1016/j.jvolgeores.2024.108029
Received 13 July 2023; Received in revised form 1 February 2024; Accepted 14 February 2024
Available online 15 February 2024

et al., 1992; Cebrià et al., 2011; Von Veh and Németh, 2009; Martí et al., 2016; Elshaafi and Gudmundsson, 2016). It is also well documented for polygenetic centered, differentiated, systems such as large-volume calderas that often lies on crustal-scale faults (Bursik, 2009 and references therein). However, the tectonic control on the transfer and emplacement of magmas in complex, polygenetic volcanic systems emplaced in evolving tectonic settings remains, from our knowledge, poorly documented.

The Mont-Dore Plio-Quaternary Volcanic Field (MDVF herein, 4.3 to 0.3 Ma) is one of such polygenetic volcanic fields as it is formed of three successive eruptive cycles: The caldera unit (3.3 to 2.2 Ma); the Aiguiller complex (2.5 to 1.5 Ma) and the Sancy stratovolcano unit (1.5 to 0.3 Ma). The MDVF lies in the French Massif Central (FMC), which was essentially inherited from the Variscan orogen (450–280 Ma; Faure, 1995; Blès et al., 1989; Vanderhaeghe et al., 2020) and then experienced from the Paleocene the establishment of the European Cenozoic Rift System (ECRIS, Dèzes et al., 2004, Michon and Merle, 2001; Merle and Michon, 2001).

The link between the Plio-Quaternary tectonic activity and the volcanism of the MDVF has long been established (Brousse, 1971; Vincent, 1980; Varet et al., 1980; Mossand et al., 1982; Brousse et al., 1990) but the precise influence of the tectonics by reactivation of preexisting

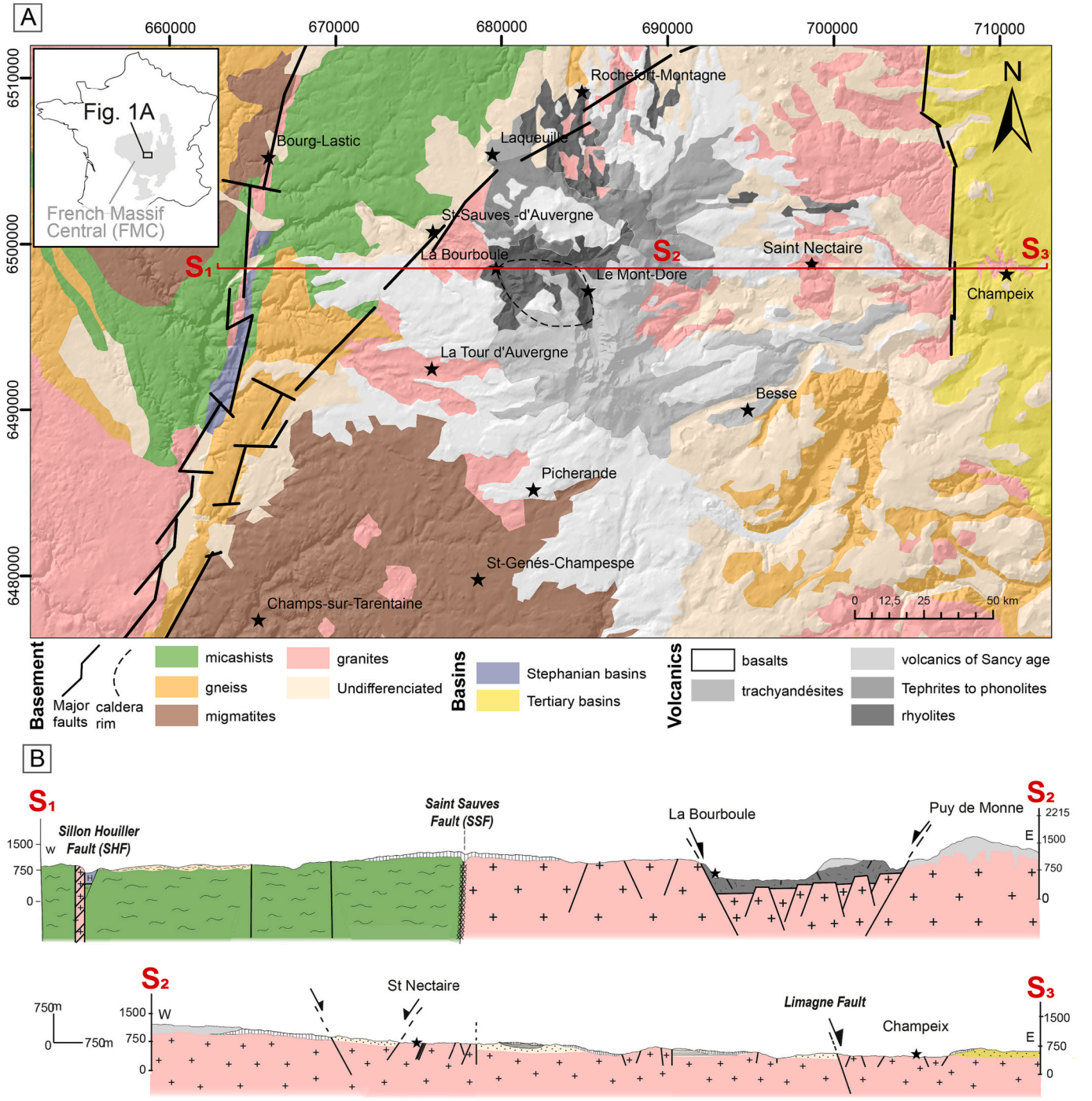

Fig. 1. A - Simplified geological map of the Mont Dore Volcanic Field area based on available 1:50,000 scale geological maps (Brousse and Tempier, 1981; Brousse et al., 1990). Caldera rim from Mossand et al. (1982). Inset map: location of the study area (box) in the French Massif Central (France). B – East-West cross section.

faults has been debated (Mossand et al., 1982; Brousse et al., 1990). Recent studies have demonstrated that during the period of the MDVF activity, the regional stress field has evolved from extensive to compressive conditions (Heidbach et al., 2016; Bellanger et al., 2019). Hence, it provides an excellent study case to document the control of the regional tectonics on volcanic activity. By combining measurements of fractures and regional lineaments in the Variscan basement, with directional analysis of dikes and volcanic vents alignments of the three volcanic units, we document how the change in faults reactivation with respect to the change in regional stress field conditions that emerged around 2.5 Ma caused an evolution in magma storage and emplacement of the Mont-Dore Volcanic Field.

2. Geological setting

2.1. he Mont-Dore Volcanic Field

The Mont-Dore Volcanic Field (MDVF) is one of some fifteen discrete volcanic fields of Cenozoic to Quaternary ages that are scattered in the French Massif Central (Fig. 1). This volcanism form part of an intraplate alkaline volcanic province, the Cenozoic European Volcanic Province (CEVP), that spreads from Spain to Poland and is spatially associated with a large-scale rift system (ECRIS) surrounding the Alps orogen. Rifting and volcanism globally formed due to local extension and mantle upwelling in response to the Alpine orogeny (Lustrino and Wilson, 2007, and references therein).

The MDVF displays a great complexity in volcano-structural and petrological respects. It is dominated by differentiated magma compositions forming both silica-oversaturated and –undersaturated suites (Brousse, 1961), erupted from a multitude of vents scattered over an area of the order of 100 sq. km. Petrological and geochemical studies have shown that the MDVF differentiation suites were mainly formed by AFC processes (Briot et al., 1991), which implies large-volume crustal reservoirs at the time, the size, geometry and depth of which are currently poorly known. Defining the MDVF as linked to the differentiation reservoir(s) (i.e. excluding basaltic vents scattered all over the MCF), its eruptive history spans a time interval of broadly 3 M.y., from ca. 3.2 Ma to 0.25 Ma, while including a few distal trachytes would put backwards the start of the MDVF activity around 4.3 Ma, based on available radiometric data (Cantagrel and Baubron, 1983; Mossand et al., 1982; Nomade et al., 2012) (Fig. 1).

Defining volcanic subunits within the MDVF has hitherto led to various schemes, mostly from the radiometric record (e.g. Baubron and Cantagrel, 1980; Cantagrel and Baubron, 1983; Cantagrel and Briot, 1990; Pastre and Cantagrel, 2001; Nomade et al., 2012). Based on geochronological, spatial, compositional criteria and our own field survey we here subdivide the Mont-Dore volcanic field into 4 units:

- The caldera unit

In the oldest period, MDVF products are mostly rhyolites, volumetrically followed by silica-oversaturated trachytes, then silica-undersaturated trachytes and less differentiated lavas. Rhyolites occur dominantly as relatively small-volume (< 10 km3 each) ignimbrites (Brousse, 1963; Brousse and Lefèvre, 1966; Cantagrel and Briot, 1990; Nomade et al., 2012; Bourdier et al., 2016). These are widely exposed in paleo-channels as far as 40 km from the central area, mainly to the North and East. Proximally, they are ponded in a paleo-depression East and South of the city of La Bourboule. The paleo-depression is geologically evidenced mostly by ignimbrite thicknesses locally >100 m and by intervening lacustrine sediments locally several tens of meters thick. Stratigraphic and compositional data currently allow to distinguish at least 5 ignimbrites and one discrete plinian airfall unit of rhyolitic compositions, ranging in age between 3.1 and 2.7 Ma (Bourdier et al., 2016 and references therein). A strong gravity anomaly broadly coincides with the paleo-depression defined geologically (Varet et al., 1980). The overall evidence has hitherto led to an interpretation of this structural depression as a collapse caldera, with conflicting proposals for its precise size, structural limits, and influence of pre-existing fault structures on its shape. Brousse (1961) defined the concept of a volcano-tectonic depression, the limit of which including the Aiguiller and the Sancy units. More recently, Varet et al. (1980) and Mossand et al. (1982), from geophysical and field evidence respectively, proposed a smaller depression that includes La Bourboule et Mont-Dore cities areas (Fig. 1).

Our stratigraphic and mapping survey (Bourdier et al., 2016) suggests that all rhyolitic plinian eruptions vented from within the caldera defined by previous authors. A few rhyolitic and trachytic lava bodies are more or less well exposed in the same area, whose available radiometric ages range between 2.6 and 2.1 Ma (Mossand et al., 1982; Cantagrel and Baubron, 1983). As a whole, the evidence is that the rhyolitic volcanism, accompanied by subordinate less differentiated magmas, (1) occurred in a restricted time interval of 3.1–2.1 Ma according to the available ages and as no rhyolitic products were emitted later in the MDVF, and (2) was erupted in a restricted area broadly coinciding with the reported Mont-Dore caldera. While the caldera remains poorly defined and is not directly addressed in this paper, we refer to this MDVF subunit as the caldera unit.

- The Aiguiller unit

In the northeastern part of the MDVF, the Aiguiller unit (Fig. 1a) is a volcanic domain dominantly consisting of lava flows and domes, and sparse proximal hyaloclastic products that are likely remnants of subglacial or sub-lacustrine tuff rings or tuff cones (Morel, 1987). Most Aiguiller magmas have differentiated silica-undersaturated compositions, namely basaltic trachyandesites, trachytes (often termed trachyphonolites in the local literature), and phonolites, subordinate oversaturated trachyandesites being also present. Available radiometric ages range between 2.4 and 1.8 Ma (Mossand et al., 1982; Cantagrel and Baubron, 1983; Morel, 1987), i.e. partially overlap the ages of the caldera unit defined above. North of the caldera unit and west of the Aiguiller unit, the Banne d'Ordanche massif (Fig. 1a) is a composite vent system and lava flow field whose age and compositions are within the Aiguiller ranges.

- The Sancy unit

In the southern part of the MDVF stands an eroded though morphologically well identifiable volcano referred to as the Sancy volcano (Cantagrel and Baubron, 1983; Lavina, 1985). This has some volcanological characteristics in common with classic composite volcanoes (stratovolcanoes), being formed of lava flows, domes and related proximal volcaniclastic deposits of mostly intermediate (trachyandesite s.l.) magma compositions. The Sancy volcano is quite younger than the above-mentioned volcanic units, radiometric ages for Sancy products ranging from 1.1 to 0.2 Ma (Cantagrel and Baubron, 1983; Nomade et al., 2012). While having volcanological features similar to composite volcanoes, the Sancy volcano is far from being a simple, well-centered structure as figured by iconic modern stratovolcanoes worldwide. Instead its central part consists of a dense network of variously trending dikes and of numerous vents from which lava flows diverge outwards, or on which lava domes are setting.

- The Massif Adventif unit

The Massif Adventif is a N010E-trending group of trachyandesite domes and adjacent volcaniclastic products that spatially connect the Sancy volcano and the Aiguiller units over a distance of about 4.5 km. With respect to magma compositions and ages, the Massif Adventif could be considered as part of the Sancy volcano. However, its specific spatial position and structural trending have led to recognize it as a

specific volcanic group since the very early studies of the MDVF (Lavina, 1985 and reference therein), and in the present work.

As a whole, the MDVF is thus a long-lived (~3 Ma) and quite dispersed volcanic complex that cannot be described as a single volcano. Most of the MDVF volcanics can be grouped into the 4 subunits defined above, which are distinct by their spatial position, age and dominant magma compositions. From field mapping, it is obvious that the products of those 4 volcanic units partly overlap, as the youngest tend to cover the older ones. However, the volcanic vents of the 4 units form discrete clusters, which allows in this study to investigate vents distribution and alignments both within the MDVF as a whole, and in each of the subunits separately. This will permit to discuss possible variations of the structural control on the vents' distribution, depending on the age and/or the spatial position in the MDVF.

2.2. The Variscan and tertiary basement

Based on differences in lithology, structures such as mineral foliation and large scales folding, and spatial relationships with crustal scale structures, namely the Sillon Houiller Fault (SHF), Saint Sauves Fault (SSF) and Limagne fault zone) (Fig. 1), seven geological domains have been identified in the Variscan basement and the Tertiary grabens around the MDVF. From the west to the east:

- *The Eygurande metamorphic unit*

In the study area, the Eygurande metamorphic unit (called Chavanon metamorphic sequence by Thiery et al., 2009; Fig. 1) is composed of alternating micashist, more or less leptynic, gneiss and migmatites. Large-scale N0140E to N160E trending fractures are morphologically clearly highlighted by the hydrographic network (l'Eau du Bourg and tributaries of Chavanon river; Brousse and Tempier, 1981).

- *The Bourg-Lastic metamorphic unit*

This unit is usually related to the Artense unit described hereafter (Thiery et al., 2009). We separated this domain as it forms a specific tectonic block bordered by the SHF to the West and the SSF to the East (Fig. 1). The metamorphic sequence is mainly composed of orthogneisses to the south and biotite-rich micaschists to the North. In the latter, the foliation is well developed. Because of the large-scale folding, with an axial plane trending N030E to N045E, this foliation strongly varies in orientation in the northeastern part of the unit. Approaching the SSF to the west, it progressively becomes parallel to this accident. N130E striking brittle faults are common in this unit and are associated to a second population mostly parallel to either the SHF or the SSF.

- *The Artense metamorphic domain*

The Artense metamorphic domain is composed of two gneiss units, which are separated by a major thrust (Brousse et al., 1990; Fig. 1). The two units exhibit a N110E to N140E striking foliation dipping 20° to 60° to the North. Locally foliation bents from N010E to N020E. A major late deformation yielded to kilometer-scale, N140E trending open folds of the foliation. Particularly developed are two major faults systems striking ~N140E and ~ N030E in the upper gneissic unit (Brousse et al., 1990).

- *The granites of the Mont-Dore horst*

Granitic plutons of various petrographical facies form most of the substratum beneath the Mont-Dore volcanics (Fig. 1). The most common facies are represented by biotite granites (La Tour d'Auvergne granite, Cournols-Saint-Nectaire granite) and two micas-bearing granites (La Bourboule granite). Due to the volcanic cover, only few major faults are observed in these granites. To the North, near the city of Rochefort-Montagne, N060E to N090E trending faults put in contact the granite with the lacustrine series of the caldera unit (Bourdier et al., 2016) pointing out that these faults were actives with a significant normal component during the upper Pliocene, or later. To the Northwest, the granite of Cournols-Saint Nectaire is affected by mostly N160E and N020E striking fractures, in particular along its contact with the Limagne basin to the west. Lastly, to the Southeast, a dense N140E to N160E faults network put in contact the two micas-bearing granite of Chambon with the lacustrine sediments of the Caldera unit (Brousse and Tempier, 1981).

- *The Saint Alyre orthogneiss*

The Saint Alyre orthogneiss is a large metamorphic formation, which extends from St Alyre and Mazoire to the North **to** the Bartonnet valley to the south (Fig. 1). Its western extension is sealed by the volcanic deposits of the Cezallier stratovolcano and it is limited to the East by the Limagne tertiary basin. This orthogneiss is affected by N135E and North-South major fractures. A secondary population is represented by N040E to N050E striking faults.

- *The Limagne Basin*

This ~North-South graben was filled by as much as 2000 m thick lacustrine sedimentation perturbed by frequent marine incursions during the Eocene and Oligocene (Michon and Merle, 2001 and reference therein, Dèzes et al., 2004; Fig. 1). ~N160E and ~N020E striking faults affect the sedimentary deposits mainly along the western border of the graben (the so-called Limagne Fault). This network is also well developed within the granitic horsts of Champeix and Saint Yvoine.

- *The undifferentiated volcanic rocks*

This ensemble is constituted of the quaternary volcanic deposits of the Chaîne des Puys to the north and of the Cezallier volcano to the south (Fig. 1). These volcanic formations were not included in this study as they are not affected by oldest brittle deformation.

2.3. Tectonic settings

Since the Visean, the Variscan basement has suffered different brittle tectonic events, which have deeply affected its structure (Faure, 1995; Blès et al., 1989; Lustrino and Wilson, 2007; Vanderhaeghe et al., 2020). The tectonic history of this basement is synthesized in Fig. 2 based on a thorough review of the literature.

During the late Variscan period (330–280 Ma), the FMC experienced one major NW-SE extension related to the *syn*-collisional evolution of the range that is only observable as ductile deformation in the lower crust units (Faure, 1995, Fig. 2). Then, a N-S horizontal shortening (combined with *E*-W horizontal stretching) that progressively rotated E-W during the Stephanian (Blès et al., 1989; Bellanger et al., 2019). This setting generated a conjugate system formed of N140E-N170E dextral and N010E to N050E sinistral strike-slip faults. This event is responsible for the establishment of the NNE-SSW crustal fault zone named « Sillon Houiller » Fault (Thiery et al., 2009; SHF therein; Fig. 1). At the end of the Paleozoic, the Variscan range was peneplaned.

During the Mesozoic, the Ligurian-Provençal ocean then the Atlantic Ocean opened, with limited effect on the brittle deformation in the FMC (Blès et al., 1989). Two successive extensional regimes occurred, a first E-W extension from early to middle Jurassic followed by a N-S extension from late Jurassic to Cretaceous (Blès et al., 1989, Fig. 2). Deformation and topographic relief formation are rather negligible during that period and the peneplain character was thus accentuated.

The tectonic activity during the Cenozoic was much more important. In the late Cretaceous and Paleocene, an intraplate compression phase with N-S horizontal principal shortening occurred, involving a buckling

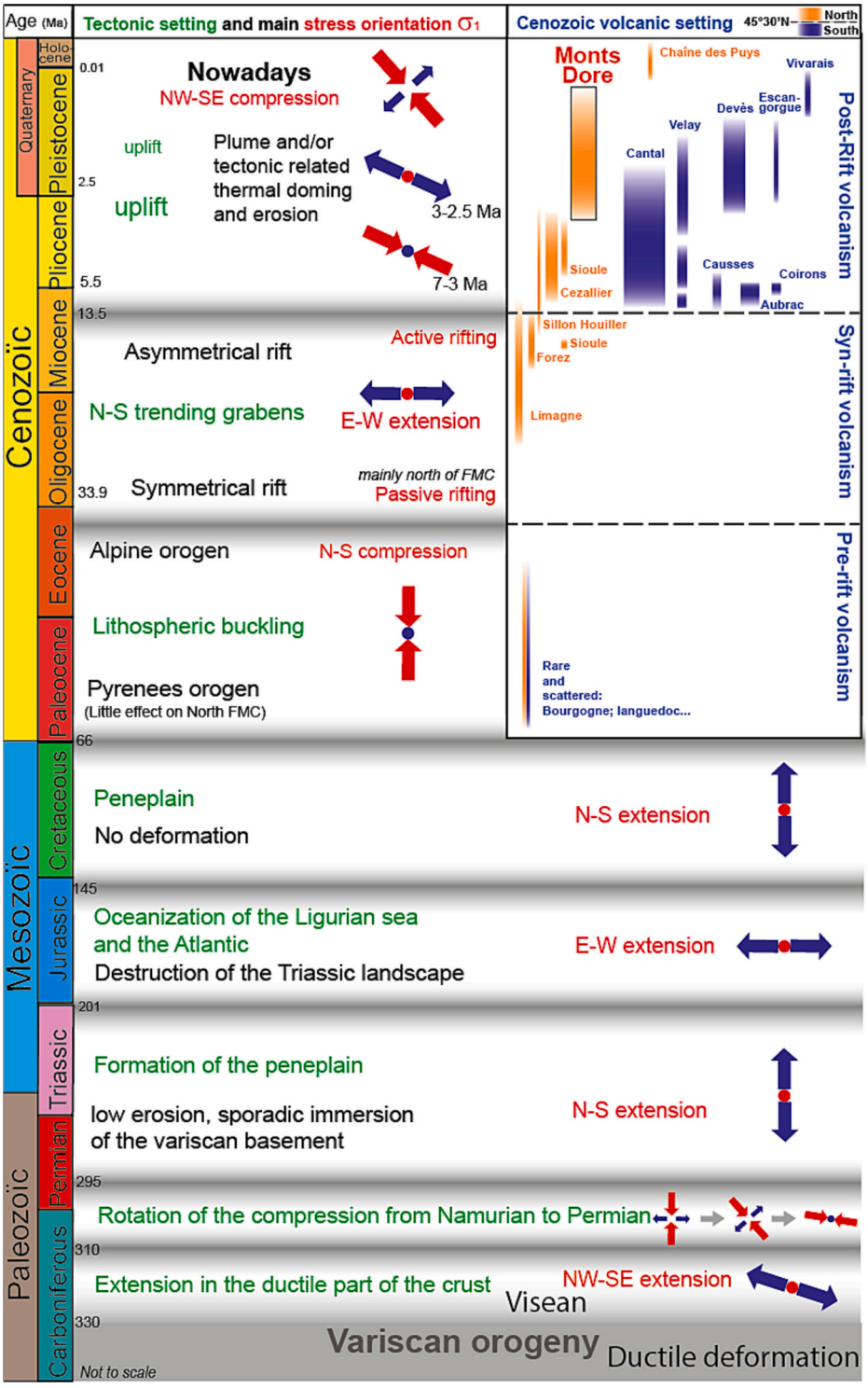

Fig. 2. Paleo-stress evolution in the French Massif central since 330 Ma. Red arrows are the principal shortening directions. Blue arrows are the principal stretching directions. Red and blue dots stand for vertical maximum shortening and stretching directions, respectively. In green are the main associated tectonic settings. Synthesis based on the studies of Bellanger et al. (2019), Faure (1995) for the late Variscan period, Blès et al. (1989) for the Mesozoic, Ziegler and Dèzes (2007) for the Early Cenozoic, and Baize et al. (2013) for the late Cenozoic. Present-day stress field from Mazabraud et al. (2005). Upper right inset: spatio-temporal distribution of the Cenozoic volcanism (modified from Michon and Merle, 2001). (For interpretation of the references to colour in this figure legend, the reader is referred to the web version of this article.)

of the lithosphere and re-activation of pre-existing crustal discontinuities (Ziegler and Dèzes, 2007). During the Eocene, this episode is followed by the establishment of the European Cenozoic Rift System (ECRIS). It is a system of about 1100 km long, composed of a fault set transect to all the Variscan massif in the Alpine foreland (Dèzes et al., 2004; Michon and Merle, 2001; Michon and Merle, 2001). The origin of the ECRIS remains debated. While Michon and Merle (2001) invoke a tectonic origin with a slab-pull model, Dèzes et al. (2004) suggested that the ECRIS is more likely related to a compression-related stress, in front of the Adriatic plate. In all cases, a mantle thermal anomaly started

during the Paleocene and caused thinning of the lithosphere beneath the FMC. The region experienced a major E-W extensive phase with the implementation of a N-S oriented graben system all around the Alpine arc (Michon and Merle, 2001). This event had a strong impact on the structuration of the region, which, until the Cenozoic, had been mostly affected by the Variscan tectonics. In the meantime, the first volcanic activities took place in the region, with rare and scattered volcanism in the North of the FMC, followed by a syn-rift volcanism mainly in the Limagne sedimentary basin (Fig. 2). During the Miocene, the post-rift volcanic phase appears at first diachronic between the south and the North of the FMC (Merle and Michon, 2001). Since the late Miocene, volcanism spreads throughout the FMC, forming the MDVF among other volcanic fields.

Two major Variscan crustal fault systems affected the basement in the study area: the Sillon Houiller Fault and the Saint Sauves Fault. The Sillon Houiller Fault (SHF) is a major lithospheric vertical, N020E trending discontinuity developed during the Variscan orogeny (Joly et al., 2007; Thiery et al., 2009). In our study area, the SHF is composed of a 250–400 m wide mylonitic shear zone formed within the Eygurande sequence and is bounded by a narrow N020E granitic sheet of 100 to 700 m wide (the Messeix monzogranite; 326 ± 4 Ma; Thiery et al., 2009).

The Saint-Sauves Fault (SSF, etheir named the Tauves-Aigueperse fault zone by Babuška et al., 2002) consists of a major Variscan crustal fault branching to the SHF, to the south, and propagating to the North-East of the FMC with a mean N045E strike. It is also recorded as a sinistral strike slip fault along its northern extension in the Morvan (Babuška et al., 2002).

3. Methodologies

3.1. Brittle structures analysis

We combined three strategies to analyze the brittle structures developed in the Variscan basement and in the Mont-Dore volcanic formations, at different scales. Small scale field measurements were combined with large scale analysis on both 1:50,000 geological maps and Digital Elevation Model (DEM) grid maps of the study area. Lineament analysis on DEMs is used to highlight potential structures that are not observable in the field and that are not shown in the geological maps. Microstructural measurements of brittle structures (fractures and faults) at selected stations yield quantitative information on local paleostresses and crosscut relationships between fractures populations.

3.1.1. Fault analysis from the geological maps

The analysis was performed on an assemblage of four sheets of the 1:50,000 scale geological map of France covering the studied area, namely n°716- Bourg-Lastic (Brousse and Tempier, 1981), n°717- Veyre-Monton (unpublished), n°740- La Tour-d'Auvergne (Brousse et al., 1990) and n°741- Besse-en-Chandesse (unpublished). Vector digital data retrieval from the digitized map files allow to create a polylines set corresponding to all of the mapped faults in the study area and to measure a weighted mean strike of each one based on the direction of their constituting segments.

3.1.2. Digital Elevation Model lineament analysis

Regional lineaments detection has been performed based on Digital Elevation Model (DEM) analysis. Indeed, lineaments can be shown as alignments of topographic highs or lows or even of slope breaks. If considering only the ones with a minimum length, such linear shapes defined as regional lineaments represent topographical features that can have various geological meanings: fracture, ductile shear zone, cleavage trajectory, contact between two lithologies or dike, depending on the spatial resolution of the DEM. The data used in this study is supplied by the French National Geographic Institute (IGN, 2011) and cover the overall study area. Data is of raster grid format as a DEM with pixel resolution of 25 m and with maximum 2.5 m vertical accuracy (IGN, 2011).

Lineaments have been manually digitized based on some filters applied to the DEM raster data and using the QGIS GIS software (QGIS.org, 2024). They include (i) artificial illumination computed for different directions of artificial light (N, NE, E, SE) to reveal lineaments, regardless of their orientation, based on the contrast of the shades of the image obtained and (ii) slope value image to highlight the most prominent effects geological structures could have on the localization of the relief incision.

It is noteworthy that the digitizing process has been performed in a range between two scale zooms in the GIS software (that was corresponding from 1:25,000 to 1:80,000 scales on the computer display) in order to detect topographic lineaments to a scale compatible with the one of the available 1:50,000 geological maps. Besides, because such manual analysis could be user dependent, a benchmarking analysis was made by comparing lineaments detection performed by different operators and only the resulting common or similar lineaments (both in location and trend of the corresponding segments) were considered for further analyses and interpretation. Finally, the strike distribution of both lineaments and of faults extracted from the geological map have been analyzed (Fig. 5). In the statistical analysis, direction of each feature is weighted to its length by computing direction of the subsegments constituting the original polylines.

3.1.3. outcrop-scale structural measurements

We conducted joints and shear fractures analysis in 12 stations distributed around the MDVF and representative of the 7 geological units defined in the basement (Fig. 3).

6 other sites were measured along two *E*-W cross sections. For each site, 50 to 114 fractures were measured. When observed, and in particular along the SHF, striae kinematics on meter-scale fault planes were measured. Low dipping joints, i.e. dipping less than about 15°, were not measured as they can generally relate to either exfoliation or unloading joints.

3.2. MDVF structural analysis

3.2.1. Directional analysis of volcanic dikes

The dikes network analyzed in this study is a combination of data from the regular geological maps, the available regional literature, and our own field measurements.

3.2.2. Spatial analysis of eruptive vents

Features identified here as volcanic vents are lava bodies of limited areal extent, whose internal structure or original shape allow to identify them as lava domes. The data set also includes a few scoria cones. For each of them, an area of uncertainty was estimated considering the uncertainty on the original extension because of erosion or partial covering by youngest volcanic products. Uncertainty varies from one feature to the other and vents can thus be represented as disks of diameters ranging from 106 to 255 m and centered on the eruption barycenter. The spatial distribution of the volcanic vents was then analyzed within each of the four volcanic units as defined above.

The spatial distribution of volcanic vents can be characterized by a degree of randomness, so that the distribution can be classified as dispersed, clustered or random. In this study, the Poisson nearest neighbour analysis is used to quantify the degree of randomness in the distribution of points by comparing their mean nearest neighbour distance of observed population (ro) with the mean nearest neighbour distance calculated from an idealized Poisson distribution (re) (Le Corvec et al., 2013). A statistical test proposed by Clark and Evans (1954) uses an R-index to measure an observed population's departure from the Poisson distribution and the c-statistical test to quantify the quality of the fit with the Poisson distribution. A population with a Poisson distribution ideally has an R values of 1 and a c value of 0. An R value >1

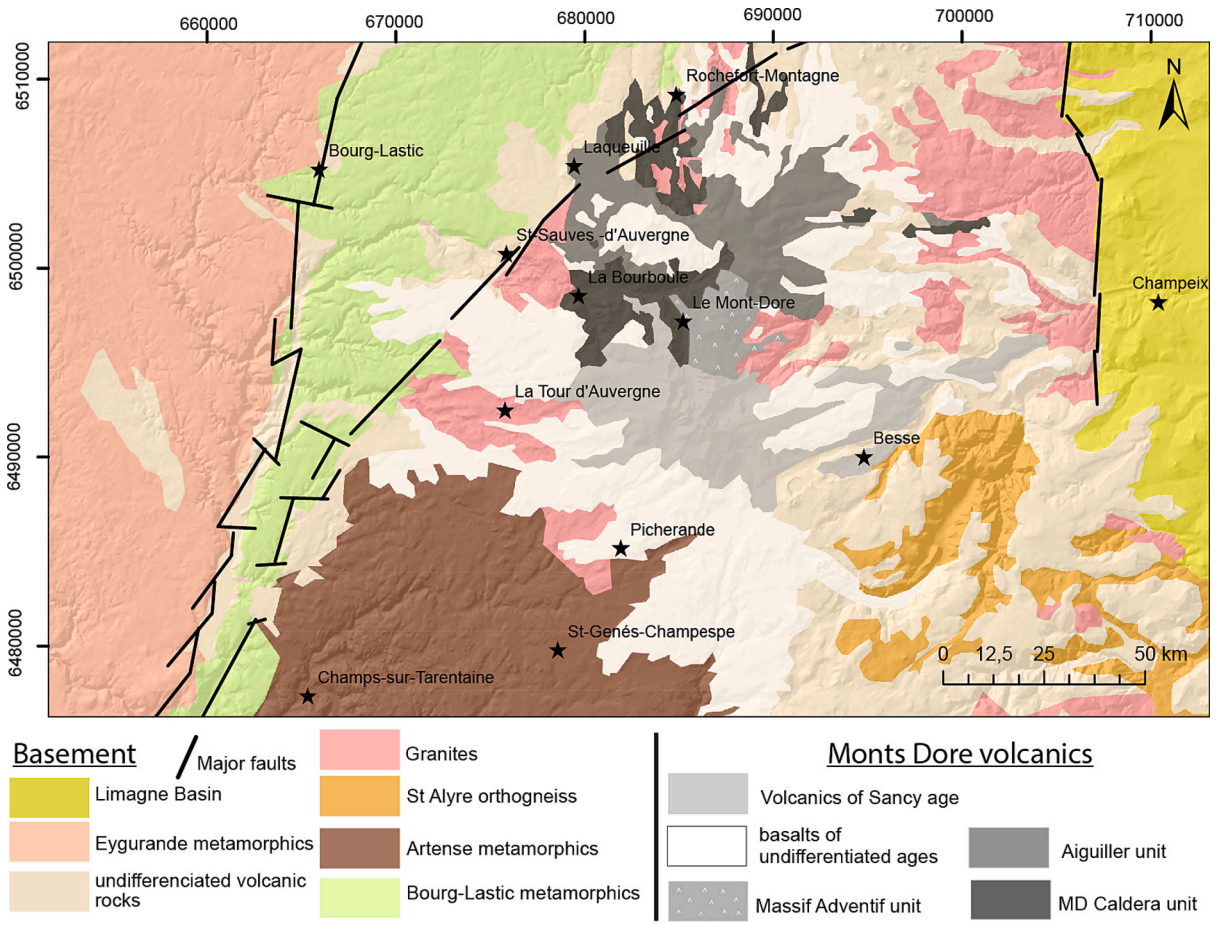

Fig. 3. Simplified geological map issued from Fig. 1 and in which each unit of both the basement and the Mont Dore Volcanic Field have been individualized. See text for the description.

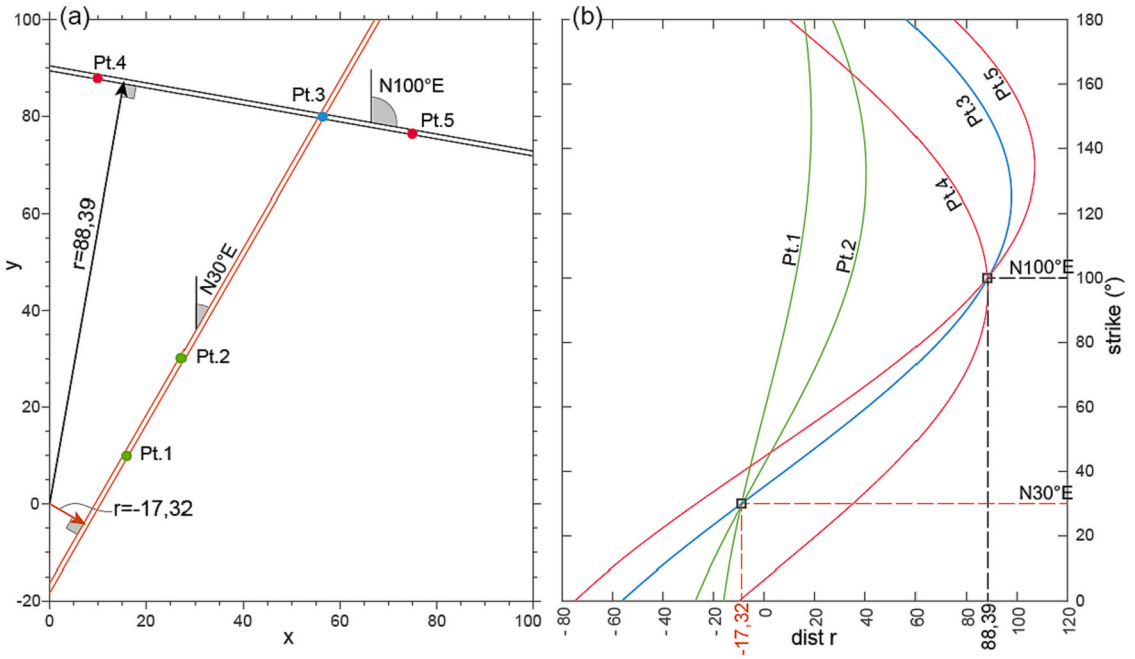

Fig. 4. The Hough transform method used to detect points alignment by image analysis. a – Example of two sets of points that are aligned at N100E (red and blue dots) and N030E (green and blue dots) respectively. b – The resulting Hough transform projection plane obtained from the map configuration in a; location and direction of the two alignments are detected where the sinusoidal curves (each corresponding to one point in the map) intersect. (For interpretation of the references to colour in this figure legend, the reader is referred to the web version of this article.)

means that the distribution is dispersed and an R value <1 means that the distribution is clustered (Beggan and Hamilton, 2010).

3.2.3. Hough transform method

The Hough transform method allows to locate and automatically trace points alignments. The Hough transform identifies alignments between points on a two-dimensional (x-y) plane, by first re-projecting the replotting points onto a plane defined by parameters (ρ; θ) (Wadge and Cross, 1988). For each point (x-y) in a cartesian map plane, an infinite number of lines with various strikes pass through and rotate on the point. Each of these lines is characterized by two parameters: the length (ρ) of the normal line drawn at a right angle between the alignment and the origin point, and the angle (θ) between the normal line and the x axis running through the origin point (Wadge and Cross, 1988). The equation of a line is given by:

$$\rho = x\cos\theta + y\sin\theta$$

Then, each point (x-y) from the cartesian map projection is represented as a continuous sinusoidal curve in the projected Hough plane and n points aligned on a same line in the map will be represented by n sinusoidal curves intersecting in (ρ1, θ1). These (ρ1, θ1) parameters correspond to the localization and the direction of the line of alignment (Fig. 4.).

This method has been automatized on MATLAB and applied to detect vents alignments. From a technical point of view, the computational process is performed through an image grid analysis mode and the map points alignments are not detected along a line but along a band of width corresponding to the cell resolution of the image (see black and red

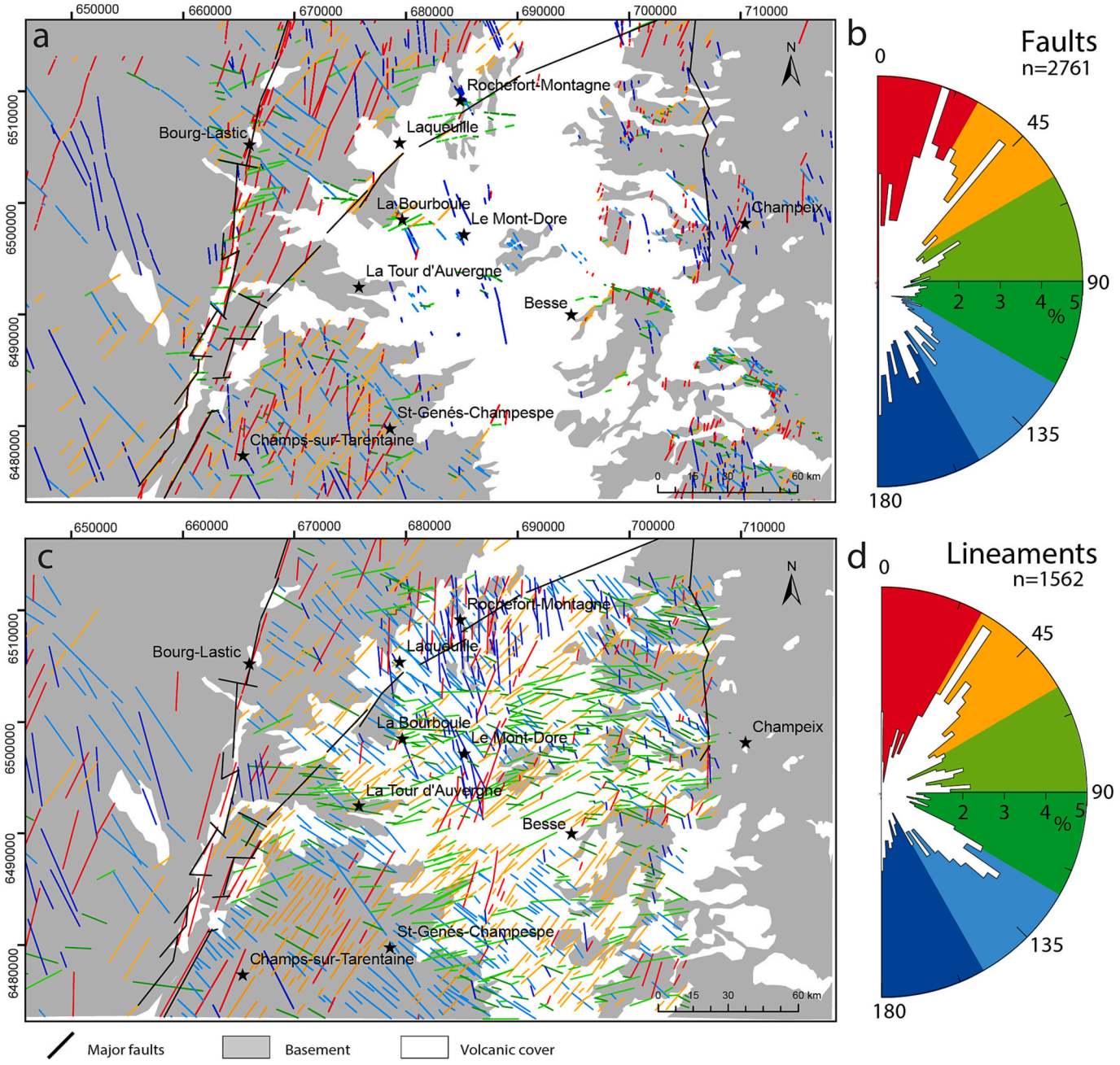

Fig. 5. Spatial (a) and azimuthal (b) distributions of the **2761** faults extracted from the 1:50,000 scale geological maps covering the studied area compared to spatial (c) and azimuthal (d) distributions of the **1562** lineaments extracted from the DEM analysis. Angular colour code division every 30°. Grey and white areas correspond to the geological units of the basement and the MDVF, respectively.

bands, Fig. 4a).

Thus, the larger is the band width used, the larger is the number of possible detected aligned points (or dots in the image). The Hough transform can therefore be considered as an exact estimator of the direction and position of the lines passing through a given number n of points in the cartesian plane (map) with the bandwidth value corresponding to the uncertainty.

4. Results

4.1. Mapped fault distribution

2761 faults were extracted from the 1:50,000 digital geological maps (Fig. 5a).

4.1.1. Faults over the study area

The distribution of the fault orientations over the complete study area shows a main population made of faults striking from N020E to N045E (Fig. 5a and b). Within this population, the N020E and N045E subpopulations clearly stand out. A secondary population is formed of faults trending from N135E to N010E and with no clear main average direction or sub-population which could be determined. It is noteworthy that the two ~N020E and ~ N160E centered populations are homogeneously represented in all the geological units.

4.1.2. Variscan basement

Distribution of faults is broadly similar over the different units of the basement and complies with the fault distribution shown over the entire area (rose diagram, Fig. 5b).

In all units the N020E direction clearly appears as a major fault

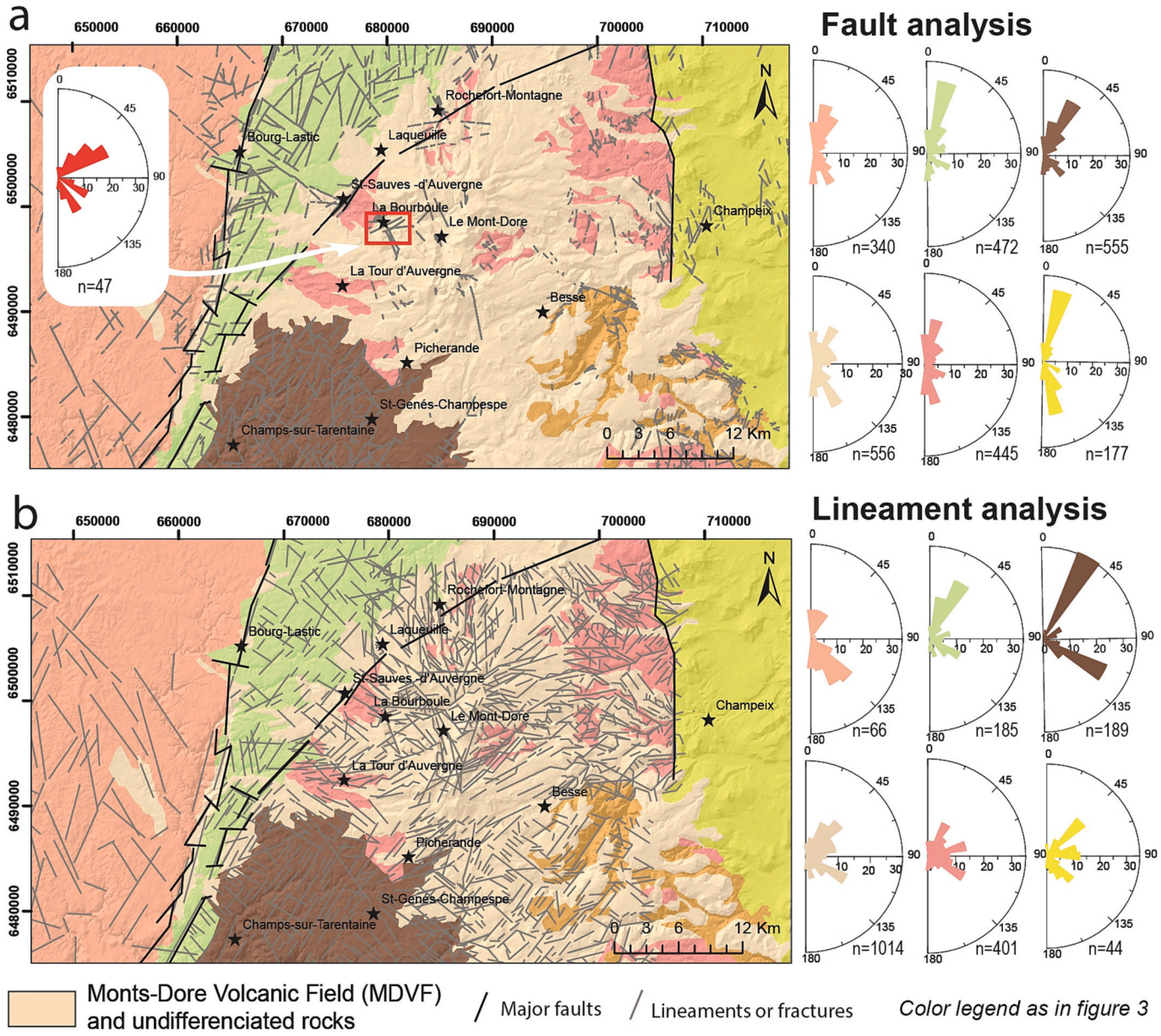

Fig. 6. a - spatial (map, left) and directional (rose diagrams, right) distribution of faults and, b - spatial (map, left) and directional (rose diagrams, right) distribution of lineaments for each domain in the Variscan and Cenozoic. The Mont-Dore volcanic units are undifferentiated. Exception comes from the inset rose diagram that represent the faults measured within the caldera unit. Note that the sum of the faults (resp. lineaments) number in each domain is larger than the total number of faults (resp. of lineaments) in the study area as a same fault's trace (resp. lineament's one) can intersect several geological domains. (For interpretation of the references to colour in this figure legend, the reader is referred to the web version of this article.)

direction (Fig. 6a). It forms the primary fault population cross cutting the Bourg-Lastic and Eygurande metamorphic sequences, the granite of the Mont-Dore horst and the western limit of the Limagne basin. In contrast, the N020E direction appears subordinate in the Artense metamorphic unit, as the main orientations comprise a N040E striking fault family. A secondary main direction comprises N160E faults in the Eygurande metamorphic sequence, the granite of the Mont-Dore horst and its MDVF cover, and the western limit of the Limagne basin. The bimodal set of the N160E and N020E trending fault populations is particularly well expressed in the latter unit. In contrast, in the Bourg-Lastic and Artense units, the secondary population comprises N130E to N135E trending faults. A last, minor, population formed of N160E to N0E trending faults is present in all basement units.

4.1.3. The MDVF volcanics

556 faults orientations have been plotted in the maps within the MDVF. The distribution of the fault orientations is similar to that observed in the underlying granitic basement of the Mont-Dore. The two main directions are represented by the N160E and N040E faults families while the third, minor N0E population is also well represented (Fig. 6a). In addition, 47 faults were measured in the La Bourboule volcanic depression and the bordering granitic basement along its western side (see red inset rectangle and rose diagram in Fig. 6a). In this restrained zone, two main orientations are clearly identified; the N050E to N060E and the N120E to N130E trending faults form the primary and secondary populations, respectively. It should be noticed that the primary N050E to N060E family is closely parallel to the SSF located three kilometers North of La Bourboule city. Finally, only few N0E trending faults were found (Fig. 6a).

4.2. Lineament analysis

1562 lineaments were recognized from the DEM analysis in the study area, including the basement and the MDVF cover (Fig. 5c). This lineament population is arbitrary divided into 6 directional classes, every 30° (Fig. 5c and d) with each colour corresponding to one class in the map and the rose diagram.

4.2.1. The lineament pattern over the study area

Unlike the faults pattern extracted from available geological maps (Fig. 5a), topographic lineaments are recognized over all geological units in the study area, including basement units and those of the volcanic cover. These also appear more evenly dispersed across the map, although some clusters do exist (Fig. 5c). Brittle structures must clearly be developed more intensely within granitic and metamorphic basement rock units that have undergone different superimposed tectonic events since the Middle Carboniferous (see Fig. 2). It is therefore logical that fewer faults may have been drawn within the MDFV units in the map and lineaments within the MDFV could thus correspond to more diffuse fracturing. Two main lineaments orientations are recognized (Fig. 5). A primary lineaments population trends N030E to N040E. This population is well represented and spatially homogeneously distributed over the basement and the MDFV cover, East of the SHF (Fig. 5d). The secondary population is represented by lineaments trending from N120E to N135E (Fig. 5d). They are well represented in all the zones of the basement. In the MDVF, this population is better observed in the western and northwestern areas (Mont-Dore, Laqueuille and La Bourboule, Fig. 5c). By opposite, N120E to N135E lineaments are nearly absent in the southern and eastern areas that cover the Sancy volcanics and the Massif adventif units (Besse, Fig. 5c). Two minor populations are also documented (Fig. 5c). A first one trending N070E to N090E as short lineaments well represented in the MDVF and in the nearby basement. Second, a N170E to N010E population is concentrated in the North of the MDVF and in the vicinity of the city of Mont-Dore (Fig. 5c and d). Finally, it should be noted that N020E lineaments remain rare, in particular along the Limagne fault where they appear as particularly short and scattered.

4.2.2. Eygurande metamorphic sequence

The number of lineaments recognized in the Eygurande metamorphic sequence, West of the SHF, is low and therefore not statistically representative ($N = 66$, Fig. 6b). However, some significative differences with the units East of the SHF can be noticed. Two main orientations are found. A primary scattered population trending between N135E and N160E is associated to a secondary N0E to N020E trending population. Very few N030E to N040E lineaments are present.

4.2.3. The Bourg-Lastic and Artense metamorphic sequences

Although they are separated by the N020E trending regional scale SSF, these two metamorphic units show similar lineament trend populations (Fig. 6b). The primary population is composed of N020E to N035E trending lineaments, i.e. mostly parallel to either the SHF or the SSF. The secondary population is composed of N130E to N140E lineaments. This latter is particularly developed in the Artense sequence (Fig. 6b).

4.2.4. The MDVF and undifferenciated volcanics

The area composed of the MDVF and of the nearby undifferentiated volcanics to the south (Picherande area), shows a large concentration of 1014 lineaments (Fig. 6b). The lineaments' distribution is comparable to the Bourg-Lastic and Artense metamorphic sequences. A well-defined N130E direction is associated to a secondary population of lineaments oriented N045E on average. However, unlike the distribution found in the metamorphic basement, the latter is much more scattered as it ranges from N0E to N080E (Fig. 6b).

4.2.5. The granites of the Mont-Dore

Because of the volcanic cover, the number of lineaments measured in the granitic basement of the Mont-Dore is low ($N = 401$, Fig. 6). The orientations found are relatively scattered but three main orientations, namely N030E, N040E and N080E are identified. They are also present along the contact between the granitic basement and the Limagne basin ($N = 44$, Fig. 6b; the lineaments have not been measured within this basin).

4.3. Basement microstructural analysis at reference sites

12 stations have been distributed (i) within all the geological units of the study area and (ii) along an overall East-West transect (Fig. 7), perpendicular to the N-S oriented Cenozoic graben system (Michon, 1999) and related regional-scale structures.

4.3.1. The Eygurande metamorphic sequence

In the orthogneisses of the Eygurande unit, the fracture network is formed of three main fracture populations almost equivalent in percentage (WSH, Fig. 7). The first population (representing 23%), is composed of N160E to N170E striking planes in which two conjugate families are recognized, both dipping 50° either to the ENE or to the WSW. The two other populations comprise N130E, and N040E to N080E striking, strongly dipping, fractures.

4.3.2. The Bourg-Lastic metamorphic sequence

Fracture measurements were performed on aluminous biotite and muscovite bearing micaschists (station X, Fig. 7). The two steeply dipping N130E and N040E striking populations found on the other side of the SHF, in the Eygurande unit, are also well represented as they form the two main populations (32% and 28% respectively). North-South to N020E sticking, almost vertical fractures, representing 18% of the measurements, form a third population (Fig. 7). This latter is parallel to the N020E trending SHF.

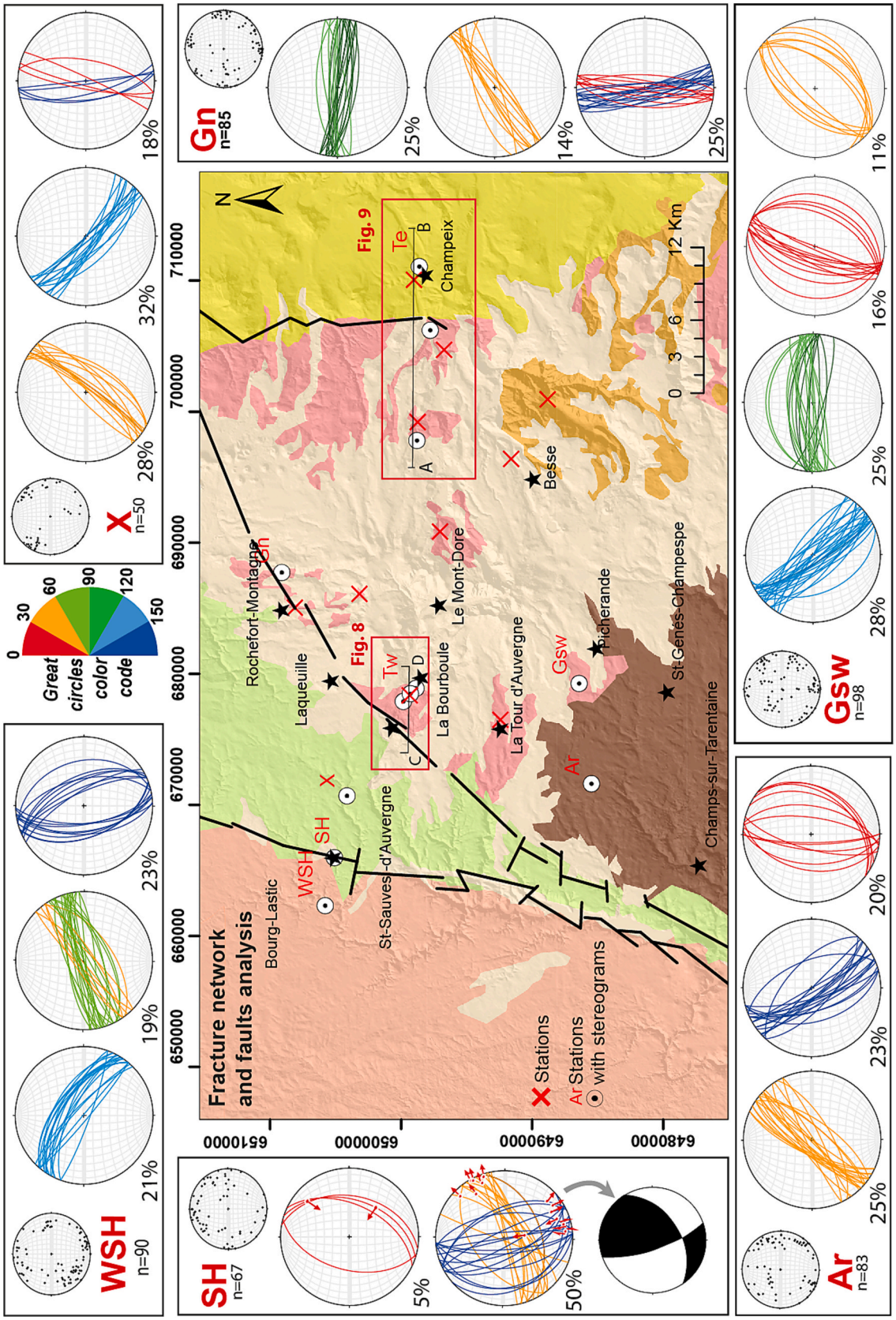

Fig. 7. Stereographic diagrams (equal area projection, lower hemisphere) of fracture populations measured in 6 sites analyzed around the MDVF. Small stereographic diagrams correspond to the poles of the full population for each site. The principal stress tensor in site SH was calculated by using FaultKin software.

4.3.3. The Artense metamorphic sequence

The station is located in a cordierite migmatite that composes the northern part of this metamorphic sequence (station Ar, Fig. 7). As in the two previous metamorphic sequences, two main associated populations composed of highly dipping fractures are identified: N040E to N060E and N160E to N170E fractures that compose 60% of the measurements (Fig. 7).

The third minor population is represented by conjugate, moderately dipping, N0E to N020E striking planes that resemble the third population found in the Bourg-Lastic sequence (station X, Fig. 7).

4.3.4. The Sillon Houiller Fault (SHF) zone

Measurements were performed in the N020E trending, Messeix granitic sheet (Thiery et al., 2009). On the basis of geometrical crosscut relationships, two families of conjugate planes were identified among the scattered planes (only 67 measurements).

The first family consists of ~N070E striking, mainly south dipping and predominantly dextral shear fractures that are associated with ~N160E striking, moderately dipping either to the East or the West, predominantly sinistral shear fractures. Analysis of fault slip from the 34 measured shear planes was performed by using the FaultKin software (http://www.geo.cornell.edu/geology/faculty/RWA/programs/faultkin.html; Marrett and Allmendinger, 1990; Allmendinger et al., 2012). The calculated stress tensor is compatible with a WNW-ESE directed, closely horizontal, principal paleo-stress direction (Fig. 7, station SH).

Because it crosscuts the previous shear fractures family, the second family appears as the youngest fractures developed in the Messeix granite. It is composed of N020E conjugate planes, gently dipping to the West and the East respectively (Fig. 7, station SH and Fig. 8a). Orientation and angular relationships point to fractures compatible with a horizontal, *E*-W principal paleo stress. However, rare and discrete slicken-lines (Fig. 7, station SH) together with crosscut relationships between the two families (Fig. 8a) point to a normal faulting component. This suggests that these shear fractures developed by a compressional horizontal field stress were reactivated later on as normal, therefore extensional, faults.

4.3.5. The Mont-Dore granitic basement

Brittle deformation of the granitic basement underlying the MDVF was measured at 8 stations. To the North, one station is located in the Fontsalade valley, South of Rochefort-Montagne city (Fig. 7, Station Gsw). To the South, one station is located near La Tour d'Auvergne (Fig. 7, Station Gsw). In addition, six other stations were selected mostly along two East-West cross sections. Three fault data sets were acquired along the Dordogne valley, along its East-west trending course, between the SSF (Saint-Sauve city), to the West, and the western limit of the Mont-Dore caldera, to the East (La Bourboule city, Fig. 9 with location in Fig. 7, transect Tw). Finally, three stations are distributed mostly along the Couze Chambon river (Fig. 10 with location in Fig. 7, transect Te).

Three families of brittle planes, also observed in the western metamorphic units, are common over the granitic basement. The two first families correspond to the N130E and N160E striking, nearly vertical, fractures. They represent the main families in the southern (Fig. 7 station Gsw), all along the western transect (Fig. 9), and in two stations along the eastern transect. These families were not observed in the eastern station of this transect possibly because of the low number of measurements on a weathered outcrop (30 measurements only, Fig. 10). In addition, the N130E family is not observed in the North (Fig. 7, station Gn). The third family comprises ~N060E striking fractures. They are generally strongly dipping excepted in the South (Fig. 7, station Gsw) where they more gently dip, either to the NW or to the SE.

Conjugate shear fractures similar to those observed in the Messeix granite (Fig. 8a) were also found in the granitic basement. N020E striking, gently dipping, conjugate shear fractures were identified as the youngest brittle event representing 12% of the measurements in the western end of the transect Te, close to the SSF (Fig. 9). Because of the intense fracturing of the outcrop, shear sense and geometrical relationships were hardly visible. Along the eastern Te transect, shear fractures were also identified. The two-family planes dip as those measured in the Messeix granite but strike N040E. Their respective orientation and their relative displacement argue also at this location for compressional shear fractures reactivated later on as low angle normal faults (Fig. 8b). Here again, these conjugate shear fractures that

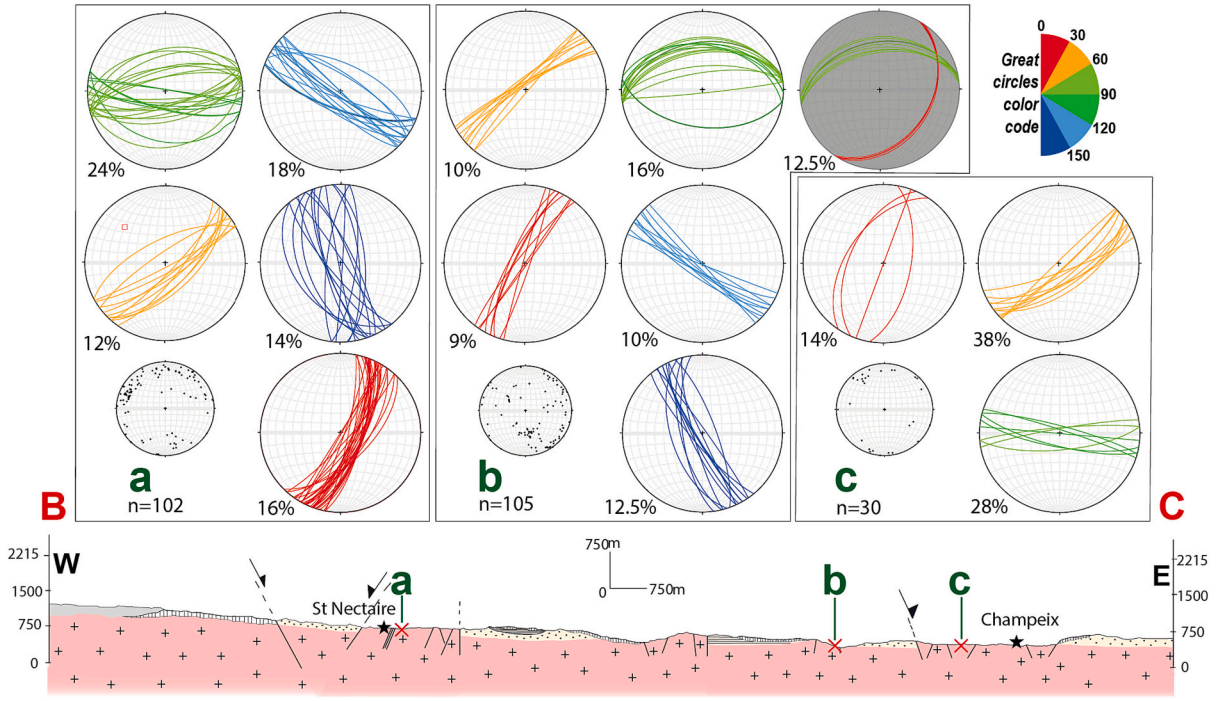

Fig. 8. Stereographic diagrams (equal are projection, lower hemisphere) of fractures populations measured in 3 sites analyzed along the cross-section Saint Nectaire -Champeix, Eat of the Mont-Dore horst. Small stereographic diagrams of the full population. The grey stereographical projection in the site b corresponds to conjugate shear fractures (see text for explanation and Fig. 10b). Locations in Fig. 7.

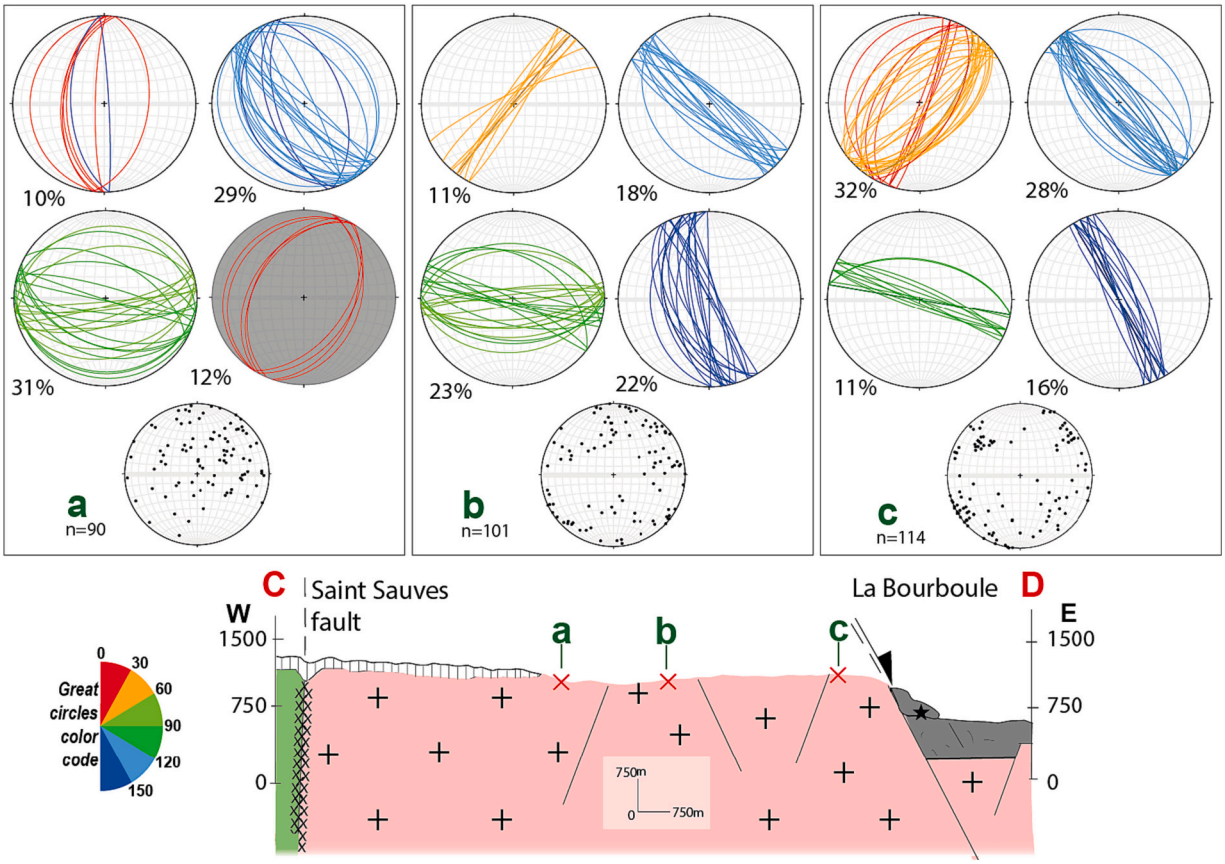

Fig. 9. Fig. 8: Stereographic diagrams (equal are projection, lower hemisphere) of fractures populations measured in 3 sites analyzed along the cross-section Saint-Sauves - La Bourboule along the Dordogne river. Small stereographic diagrams show poles of the full population. The grey stereographical projection in the site a corresponds to conjugate shear fractures (see text for explanation and Fig. 10a). Locations in Fig. 7.

represent 12% of the whole measurements, are the youngest brittle events.

With respect to the fracture populations measured in the western metamorphic units, three additional populations were found in the granitic basement. The most represented one (11% to 31% of the data set), is formed of ~E-W striking fractures. They are present in all stations. They are composed of vertical planes in the North and in the South of the granitic basement (Stations Gsw and Gn, respectively; Fig. 7). Along the two E-W transects, these fracture populations evolve from vertical to a gently dipping attitude. In particular, along the western transect Tw (Fig. 9), N090E to N100E planes are vertical in the vicinity of the Mont-Dore caldera (station c, Fig. 9), while they progressively tend to gently dip, and even become flat, approaching the SSF (station a, Fig. 9). The second additional population is represented by N-S to N010E striking, vertical fractures. They are particularly developed in the northern area of the granitic basement (25% of the population, station Gn, Fig. 7) and are also present to a lesser degree at the western margin of the Mont-Dore Caldera (Fig. 8c). Finally, the last new brittle population observed in the granitic basement is made of N020E striking fault systems. They are composed of 4 to 8 parallel, eastward highly dipping, normal faults (Fig. 8d). These normal fault systems were exclusively found from place to place, along the eastern Transect Te between Saint Nectaire and Champeix (Fig. 10). They are particularly well exposed in the station b (Fig. 10) where field evidence shows that they represent the youngest brittle event at the outcrop scale. Unfortunately, no field relationships were found with the N020E gently dipping conjugate shear fractures in order to decipherer their relative ages.

4.4. Dike orientation analysis

Directional data sets for the volcanic dikes were acquired for the Mont-Dore caldera unit (66 measurements), the Aiguiller unit (9 measurements) and the Sancy unit (50 measurements). All the dikes observed in the field are mostly vertical, or highly dipping. Therefore, only the strikes of the measured dikes are considered (see polar histograms, Fig. 11).

In the Mont-Dore caldera unit, most dikes crosscut the ignimbrites deposits and the interlayered lacustrine sediments. Two main orientations are found. First, N040E striking dikes are present throughout the area but they are particularly concentrated along a corridor trending from the South to the East of La Bourboule (Fig. 11). Second, N080E to N090E striking dikes are mostly located North of La Bourboule. A minor population constituted of N130E to N160E striking dikes was recognized in our field work, in particular in the Vendeix Valley.

Because of the poor data set, a statistical analysis of the dike orientations in the Aiguiller Unit cannot be performed. Most are N0E to N020E striking dikes (Fig. 11).

In the Sancy unit, the data set used comes from field measurements by Lavina (1985). Although trending orientations of the basaltic to trachy-andesitic dikes are relatively scattered, and particularly in the central part of the edifice, two main orientations can be distinguished (Fig. 11). N115E to N130E striking dikes are well distributed over the Sancy Massif, while N0E to N020E striking dikes are mostly localized in its eastern area (Chaudefour Valley), and especially toward the Adventif massif to the North-East (Fig. 11).

Fig. 10. N020E striking normal faults systems affecting the underlying basement of the MDVF. All views look to N020E. A and B: conjugate low dipping reverse shear fractures attributed to a NW-SE directed horizontal compression. White arrows point the subsequent, similarly directed, normal movement. A – a conjugate set of shear fractures affecting the Messeix granite emplaced along the Sillon Houiller Fault (Station SH, Fig. 7); B – conjugate sets of shear fractures affecting the Saint Nectaire granite East of the city of Champeix (grey stereogram of site b, Fig. 8). C – set of East dipping normal faults (red stereogram of site a, Fig. 8) at the edge of the city of Saint Nectaire. D – dense network of vertical fault crosscutting the La Bourboule granite bordering the caldera unit (Fig. 9, location c, La Roche des Fées hill). (For interpretation of the references to colour in this figure legend, the reader is referred to the web version of this article.)

4.5. Vents distribution and alignments

The eruptive vents identified in the MDVF comprise phonolitic to trachy-phonolitic, trachy-andesitic to trachytic and rhyolitic lava domes or lava flow vents. The mafic volcanism (Basaltic vents, either scoria cone remnants or nec) is ubiquitous in the FMC and remains until now mostly undated. Therefore, because the basaltic vents cannot be readily linked to one of our 4 volcanic units, they were not included in the lineament analysis, and the data set results in 74 "non basaltic" eruptive vents as displayed in Fig. 12.

4.5.1. Vents map distribution

The DNN (randomness) ratio over the entire MDVF is $R = 0.918$, which highlights a quasi-random ($R = 1$) dispersion with a very limited clustering tendency throughout the area. Such random distribution is well adapted to use the Hough transform method to automatically detect potential points' alignments; this approach is applied to the recognized eruptive vents.

The uncertainty radius in the location of the eruptive centers recognized in the study area ranges from 106 to 255 m (151.3 m on average). Therefore, in order to get a representative number of vents' alignments with no over-estimation and considering the minimization of the noise due to this location uncertainty, bands have been restricted to 100 m width for the Hough transform analysis. This represents ~0.5% only of the larger width of the map extension considered for this computation.

4.5.2. Vent alignments

When considering the overall 74 vents of the MDVF, two major alignments of six vents each trend N010E and N020E (Fig. 13a). Associated to these alignments are three secondary alignments composed of 5 vents and that trend N015E, N035E and N160E respectively. All are almost centered on the Sancy and the Adventif units. In addition, several alignments of either four and three vents were extracted and analyzed separately for each volcanic unit, as follows.

Two alignments of 4 vents each and trending N060E and N110E respectively are found within the Aiguiller unit (Fig. 13c). Several secondary alignments of three vents are also evidenced. Trending orientations of most of them range from N070E to N110E while three N020E trending alignments are identified in the eastern edge of the Aiguiller unit, North of the Adventif unit (Fig. 13a and c). Three alignments of either four and three vents among the fifth alignments clearly trend N020E in average (Fig. 13d). Two principal classes of orientations are observed in the 22 vents of the Sancy unit. The two major alignments composed of four vents trend N020E and N130E respectively. In addition, alignments of three events compose two groups oriented N020E to N050E and N100E to N135E respectively.

5. Discussion

This study presents results of a new structural analysis of the MDVF and its surrounding basement, at different scales. It combines (i) direction statistics of faults mapped at 1:50,000 scale, (ii) regional-scale lineament extraction and (iii) local-scale statistical analysis of fractures orientations for some selected localities. For scale consistency, the topographic lineaments extraction has been performed to scales ranging from 1:25,000 to 1:80,000 which includes the 1: 50,000 scale of the available digital geological maps and corresponding faults features. It is

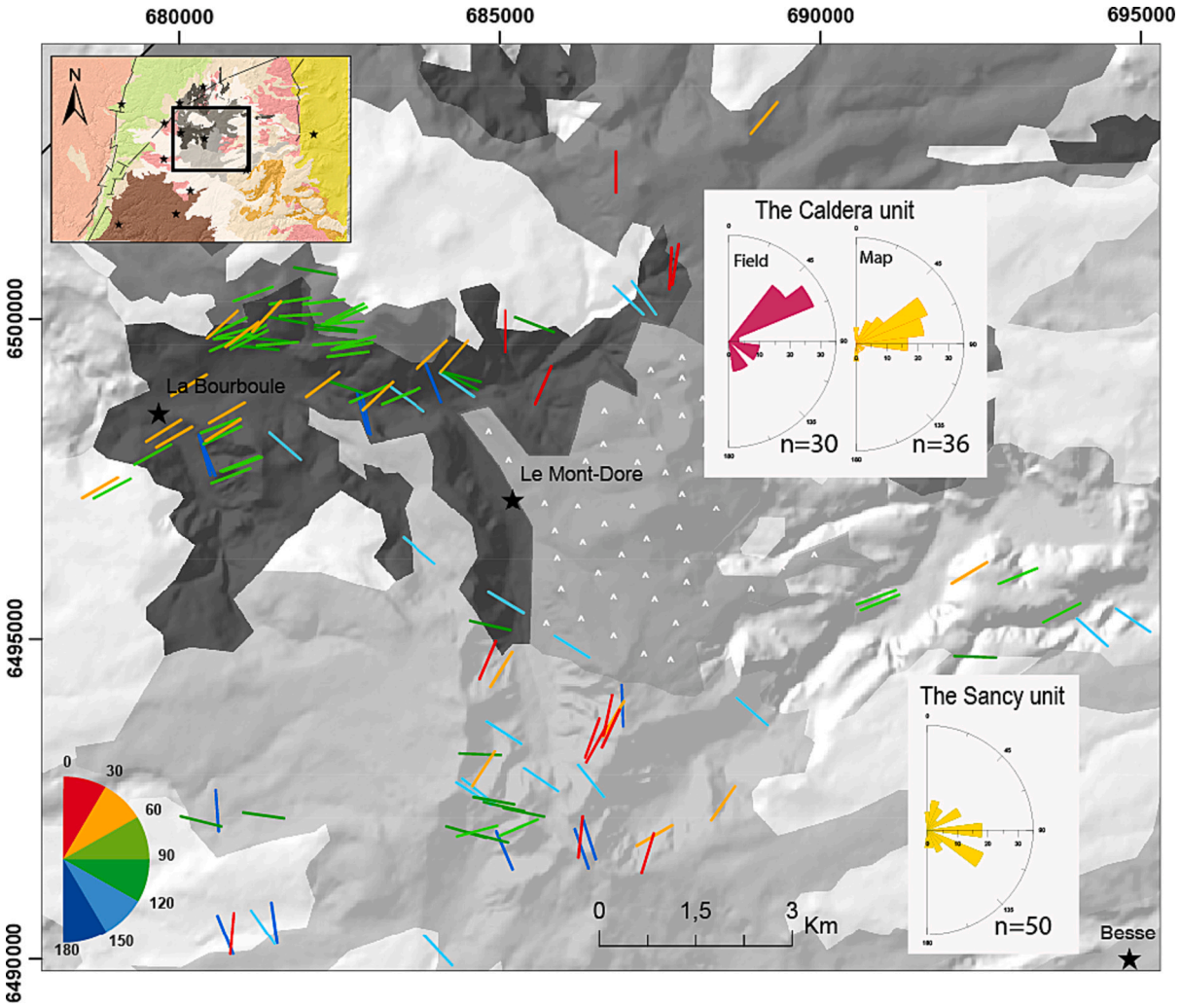

Fig. 11. Position and orientation of volcanic dikes over the MDVF (same colour codes as defined in Fig. 5). In the caldera unit (darker grey), 36 dikes measurements come from the geological maps of Brousse and Tempier (1981), and Brousse et al. (1990) combined with 30 new field measurements (this work). 50 measurements in the Sancy units from Lavina (1985).

noteworthy that lineaments extraction has not been performed at higher scale than 1:25,000 and no lineament of <1 km long are thus considered in this study. This allows to avoid highlighting local topographic effects which could originate from anthropic activity and that only the regional-scale topographic lineaments are considered which more certainly result from geological/structural controls. Besides, the structural analysis of the Variscan basement units, where both lineaments and faults have been measured, clearly shows parallelism between the mapped faults and the lineaments extracted from this analysis (see below). 3D fault orientation analysis has been performed at outcrop-scale in order to better constrain the tectonics associated to the brittle structures' activation. The 12 stations have been selected (i) to sample all the geological units of the study area and (ii) for their particularly good outcrop conditions and representativeness of the overall respective units. Statistical results show comparable orientations between these outcrop-scale structural measurements and the directions obtained from the analysis of map-scale faults within the corresponding geological unit (see Fig. 6). Besides, brittle structures are compared to the distribution and orientation of magmatic eruptive vents and dikes, respectively. The Hough transform method allows to detect eruptive vents alignments throughout the overall study area. Given a 100 m uncertainty (i.e. ~0.5% of the study area width), based on the uncertainty of the eruptive vents location (Fig. 12), this automatic approach highlights that vents aligned along the main map-scale structures.

As detailed below, this new structural multi-scale analysis allows us discussing the influence of the brittle structuration of the Variscan basement units on the MDVF volcanism distribution over time, while regional stress changed.

5.1. *The brittle heritage of the basement*

5.1.1. *The Variscan heritage*

Our structural analyses at various scales of the brittle structures affecting the Variscan basement highlights the existence of four main orientations that can be related to the late-variscan brittle events. First, the main couple of orientations consists of N020E associated with N160E faults, lineaments and fractures. They constitute major Variscan orientations well known over the FMC (Faure, 1995). Indeed, an intense network formed by N020E/N030E and N160E orientations affects the Saint Alyre gneisses and the Monts Dore granitic basement (Fig. 6; Michon, 1999). N020E orientations are also well represented as lineaments and faults all along the major Variscan accidents that are the SHF and the southwestern branch of the SSF (Figs. 5 and 6). A third direction evidenced in our structural analysis is N130E. This constitutes the main lineaments population, together with the N020E direction, in the Artense units (Fig. 6a). This over-representation of N130E lineaments in this unit is certainly explicable by the control of gneissic foliation fabric and the kilometric scale folding, all striking N110E to N140E (Brousse

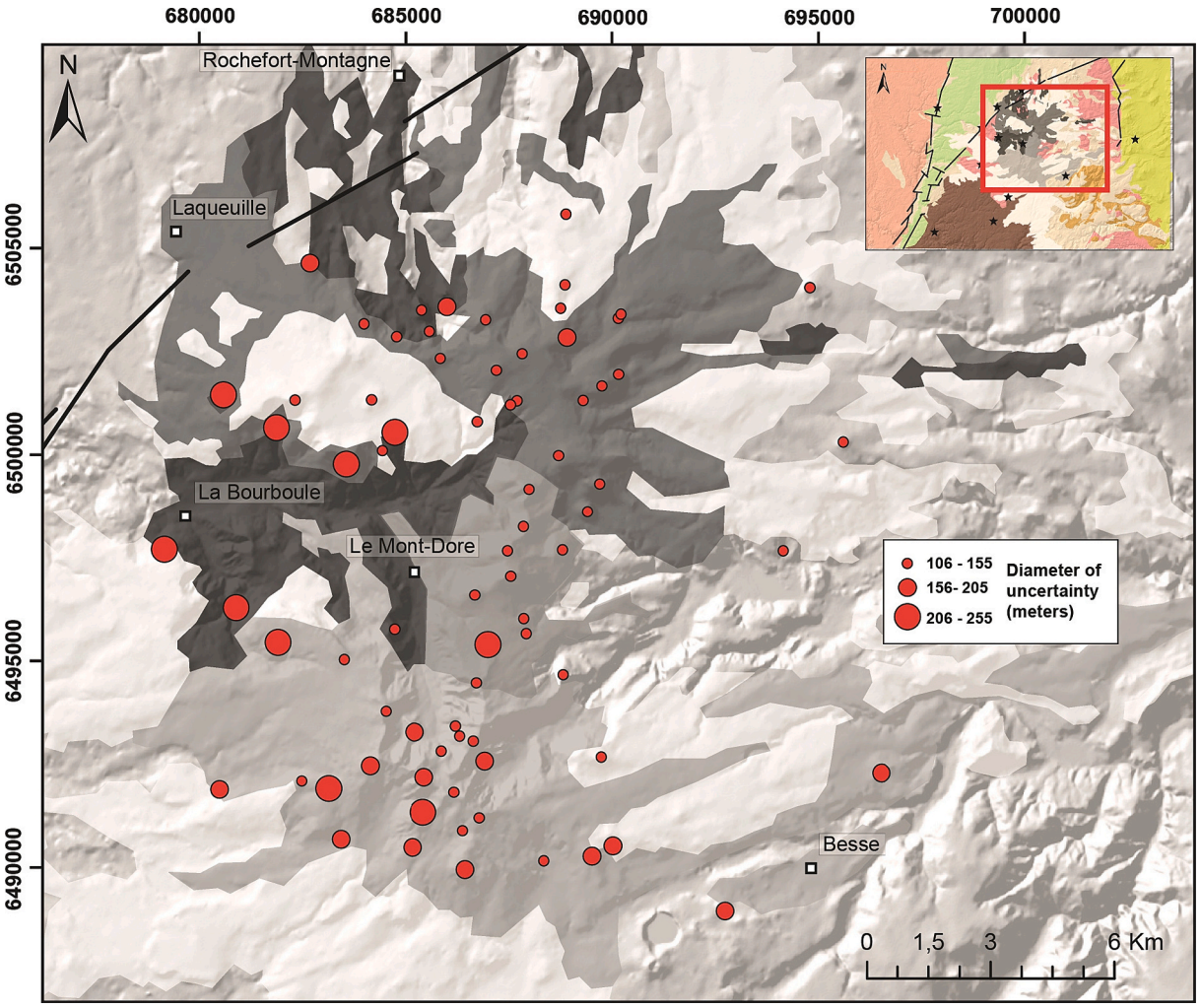

Fig. 12. Location and diameters of uncertainty of 74 volcanic vents identified over the MDVF based on Brousse and Tempier (1981), Brousse et al. (1990), Lavina (1985) and our field work. Because of their limited number, vents related to the Caldera unit are not considered.

et al., 1990), on the hydrographic network. Surprisingly, while N130E orientations constitute the second main population of lineaments measured over the studied area (Fig. 5a and b) they are little represented in the fault population measured on the geological maps (Fig. 5c and d). Finally, the last main population that emerges from our analysis is composed of the N080E to N090E orientations. This mainly affects the granitic basement underlying the MDVF as fractures and faults (Figs. 7, 8 and 9) and it stands out also in the lineament analysis (Fig. 6a).

5.1.2. The Oligo-Miocene and Pliocene brittle reactivation

The European Cenozoic Rift System (ECRIS) emerged during the late Eocene by reactivation of these Variscan, Permo–Carboniferous and Mesozoic crustal-scale faults in an *E*-W extensional tectonic setting (Fig. 2, Fig. 14a). It caused the formation of the Limagne graben in the region (Blès et al., 1989; Michon and Merle, 2001; Fig. 14a) in response to a crustal thinning down to about 23 km below the Limagne-MDVF area (Bergerat et al., 1990). This first stage of the ECRIS has reactivated mainly as normal faults the preexisting N20 and N160 striking Variscan faults (Merle et al., 2023; Fig. 14a).

During the early Pliocene, the regional differential stress evolves progressively toward a NW-SE compression (Fig. 14). This post-rift tectonic phase is characterized by a regional uplift in response to both the isostatic equilibration of the thinned crust and the change of the main stress direction (Michon, 1999; Merle and Michon, 2001; Westaway, 2004; Ziegler and Dèzes, 2007; Merle et al., 2023). As a consequence, N020E and N160E Variscan faults continued to be reactivated with a normal relative movement while, newly formed set of parallel, East dipping, N020E normal faults may have significantly participated in this vertical accommodation (Fig. 10c). In addition, compressional N020E to N040E striking and low dipping shear fractures observed over the studied area as the youngest brittle structures, were presumably formed during this tectonic event. However, because of the low displacement recorded in these planes, their contribution to the regional stress accommodation during the upper Miocene was probably trivial.

During the upper Pliocene, the regional stress field led to a NW-SE extension (Ziegler and Dèzes, 2007; Fig. 2, Fig. 14). The regional uplift in response to the thermal doming became significant. N020E and N160E normal faults continued to accommodate the vertical movement on the western and eastern side of the granitic horst (Fig. 14). Because of this changing regional stress field, newly generated N080E to N090E normal faults developed on the northern side of the granitic basement. Despite the lack of evidence for the presence of equivalent south dipping faults in the southern area close to Besse city, a pyramid-shaped horst, probably centered beneath the present-day Adventif and Sancy units positions, build-up. This is in this context that the differentiated products of the caldera unit were erupted.

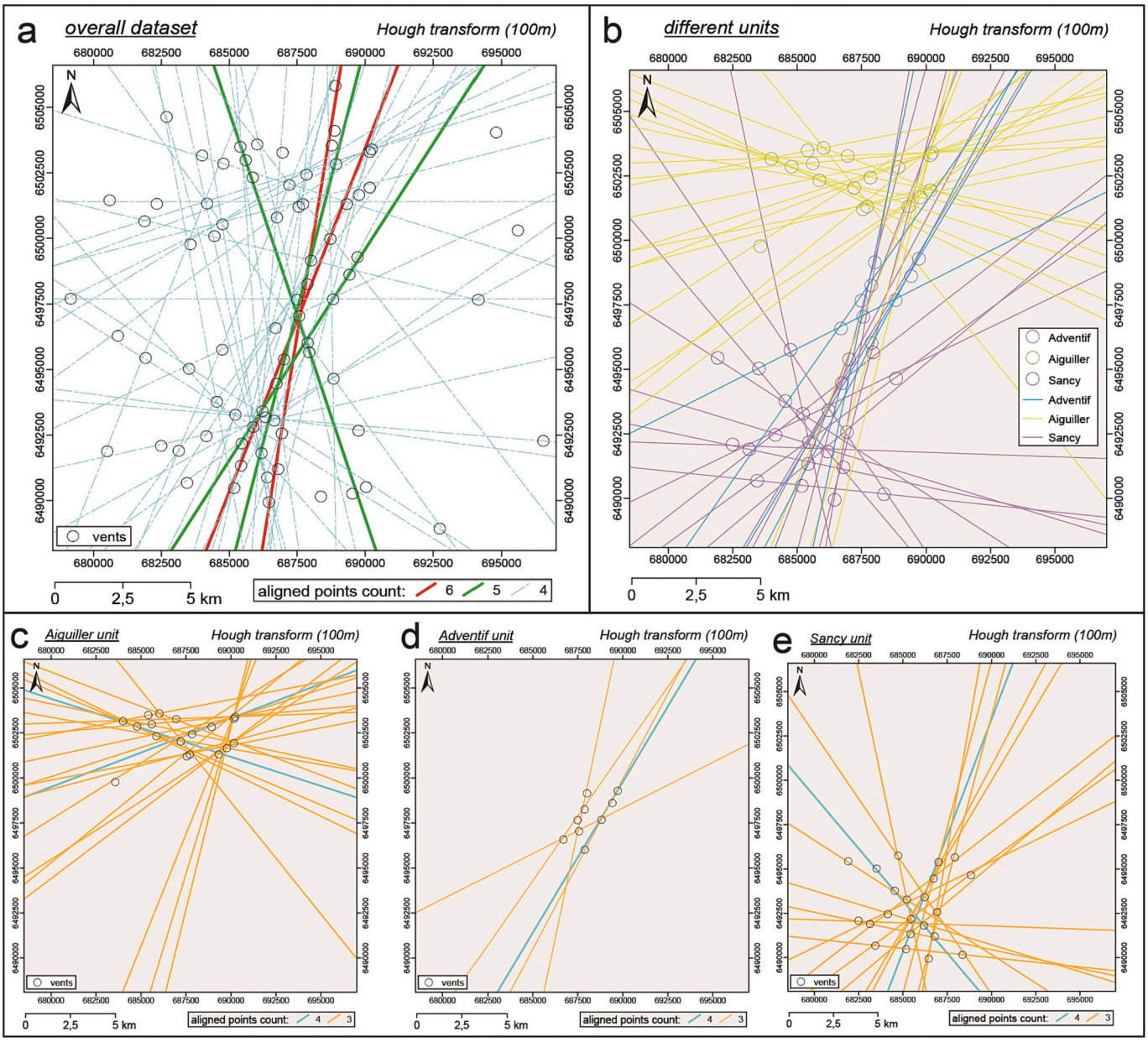

Fig. 13. Hough transform analysis highlighting vent alignments throughout the MDVF with a band width of 100 m applied (see text for further explanations). Circles showing location of the center point of the eruptive vents considered (see Fig. 12) with no indication of location uncertainty given here. a – Hough transform resulting map for all the 74 vents; only alignments of 4 (light blue), 5 (green) and 6 (red) points (vents) are plotted. b – Alignments obtained by the Hough transform method applied separately on eruptive vents from the Adventif (blue), Aiguiller (yellow) and Sancy (purple) units. Colors of the alignment lines correspond to the one of the vents' points in the corresponding massif. c, d and e – Hough transform applied to the eruptive vents of the, respectively, Aiguiller, Adventif and Sancy units taken apart. Light blue lines correspond to the alignment of 4 eruptive vents and the yellow ones to 3. (For interpretation of the references to colour in this figure legend, the reader is referred to the web version of this article.)

5.2. Tectonic control on the MDVF activity

5.2.1. The caldera unit

The extension and shape of this depression remain both elusive as its southeastern extension is actually largely covered by the younger lava and pyroclastic flows of the Sancy sequence (Brun, 1975). It is likewise debated that pre-existing fault structures affecting the granitic basement could have had a potential influence on the shape of this depression (e.g. Brousse, 1971; Vincent, 1980; Varet et al., 1980; Mossand et al., 1982). Our detailed structural measurements in the granitic basement near La Bourboule in the vicinity of the caldera rim, together with measured orientations of faults and volcanic dikes crosscutting the volcano-sedimentary sequence that filled the caldera, yield some constraints. The contact between the ignimbrites and the granite near La Bourboule city is formed by N010E to N060E normal faults and N130E faults, their association forming a dihedral-shaped rim at the decametric scale (Fig. 9c and 10c). Along the Saint Sauve-La Bourboule cross-section (Fig. 9), North of the caldera, three main orientations were observed: N040E, N130E to N160E, together with a minor N110E direction. All show large dip variation close to the SSF, where they appear clearly Variscan in age, while they all progressively become nearly vertical approaching the caldera's border. This suggests that all these orientations were reactivated as vertical faults during the formation of the depression. West of the caldera, the orientations N040E to N060E, that are absent to the West, develop substantially when approaching the depression rim. Some of them that dip to the South-East acted as normal

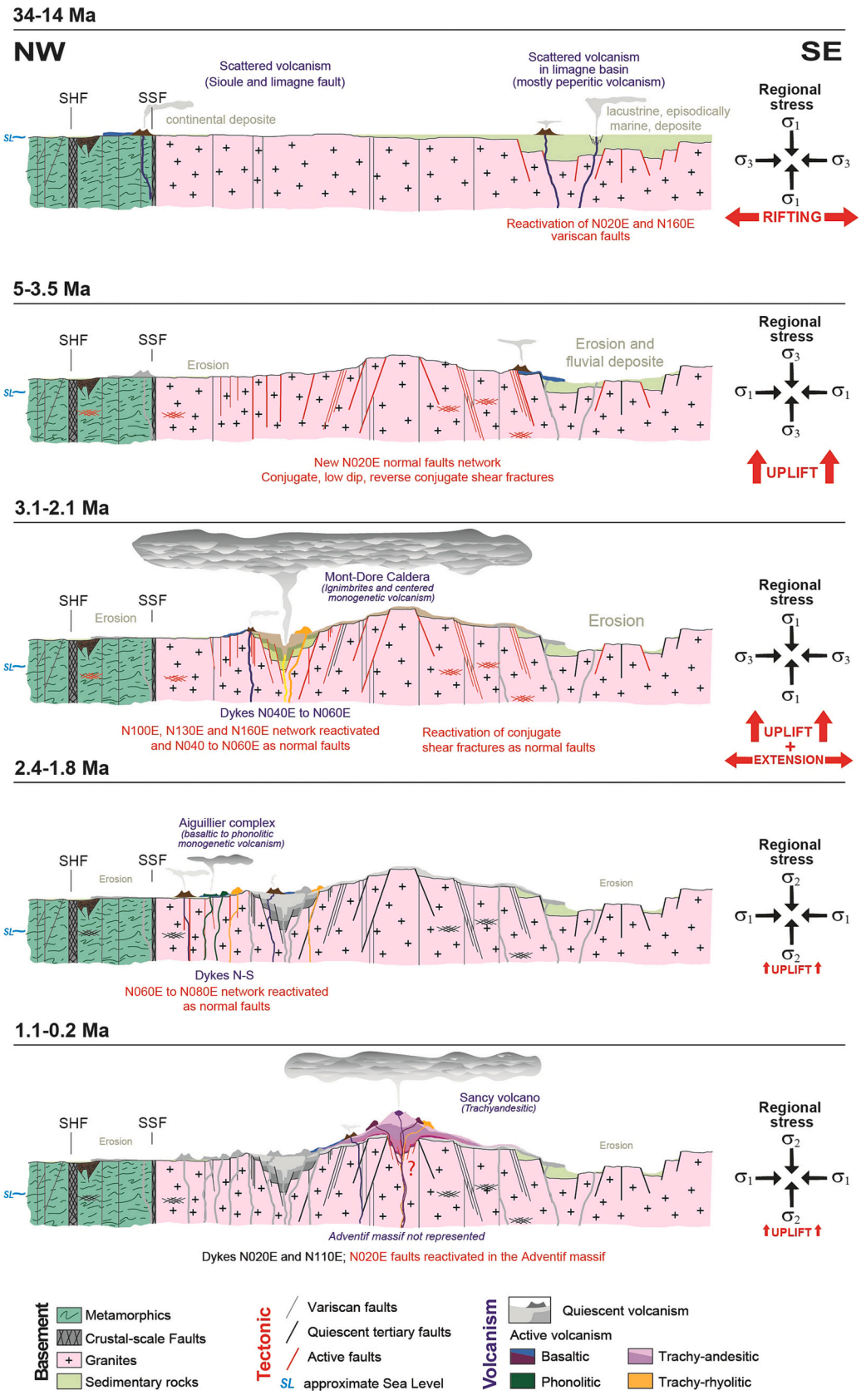

Fig. 14. Volcano-tectonic evolution of the Mont-Dore Volcanic Field. Volcanic structures modified from Cantagrel and Baubron (1983) and Gourgaud (2016). Variscan basement based on the geological maps of Brousse and Tempier (1981) and Brousse et al. (1990). Stress fields from Ziegler and Dèzes (2007) and Bellanger et al. (2019).

faults and could be related to the same family planes than the conspicuous normal fault mirror plane exposed behind the Choussy thermal baths (Brousse, 1971). In addition, the northern area of La Gacherie rhyolitic dome that emplaced within the depression is crosscut by a dense network of N080E to N090E, and accessory N060E, dikes (Vincent, 1980; Brousse et al., 1990). This suggests that the northern side of the depression in this area may be located beneath the northern side of the La Gacherie dome and was structured by reactivation of the preexisting N080E to N090E accidents in the granitic basement.

Within the caldera, N060E, N135E, and secondary N160E, *syn*-sedimentary faults affect the lacustrine series emplaced during the quiescent interplinian period. Meanwhile, most of the dikes crosscutting the ignimbrites deposits and their interlayered lacustrine sediments strike N060E, with a secondary direction close to N160E. The major N160E lineament recognized in this volcano-sedimentary sequence and that correspond to the Vendeix valley axis is likely attributed to a reactivated crustal fault (Varet et al., 1980). The Monneron dome, one kilometer East of La Bourboule, is connected from its northeast side with a N060E striking dike (Brousse and Tempier, 1981) and it is also crosscut by a similarly oriented fault.

All evidence thus suggests that the NW-SE extension that prevailed during the caldera unit activity (3.1–2.1 Ma, Fig. 14) reactivated Variscan N060E to N080E and N135E orientations in the intensively fractured granitic basement. N060E to N080E orientations acted as tensile fracture or normal faults and were the main drains for the magmas near the surface in particular as newly formed brittle structures within the volcano-sedimentary sequence filling the caldera, while strike-slip movement along N135E faults accommodated predominantly the NW-SE extension. The caldera unit is related to the largest differentiation reservoir that was active during the MDVF volcanism. A dihedral shape of the reservoir might have been controlled by these two orientations. Briot et al. (1991) proposed a model in which basaltic magmas issued from partial melting of the upper mantle migrated through opened fractures in the granitic basement. Following the model of Feybesse and Lespinasse (1987), they proposed that basaltic magmas concentrated along N135E striking, East dipping faults along with they formed a dense anastomosing network of melt-rich pockets that promoted extensive assimilation of the granitic country rocks (12–15% of assimilation, Briot et al., 1991). They further proposed that melt-rich fractured zone was continuously filled by ascending primary basaltic melts, leading to a large magmatic chamber at a shallow depth of 1 to 5 km (Ménard et al., 1980). Our study suggests that N060E were also major drains, at least at shallow depth. The intense thermal doming, together with NW-SE extension, probably enhanced the formation of a shallow magma chamber possibly by providing the creation of accommodating space as often invoked for rhyolitic volcanism emplaced in extensional settings (Bursik, 2009). N020E to N050E striking, shear fractures, recognized as the youngest brittle phase (Fig. 8b and 10b) that acted during the Miocene, may have been reactivated during this late Pliocene extensive phase as normal low dipping faults, as they are actually observed (Fig. 10a and a). If so, they could represent a third family plane that could have formed the root of the reservoir.

Finally, Carlino et al. (2014) suggested that ash-flow calderas developed under an extensional regime may progressively collapse without involving only any significant catastrophic collapse related to the Plinian eruptions. In the caldera unit, this hypothesis is supported by the abundance of syn-sedimentary faults developed during the quiescent volcanic phases observed in the intra-plinian lacustrine deposits. This tectonic effect might have added to the possible collapse of recurrent syn-eruptive small calderas. Cumulating eruptive and tectonic processes could might explain the apparent discrepancy between the relatively large size of the gravity anomaly and of the caldera as previously proposed (Brousse, 1963; Mossand et al., 1982) and the small cumulative volume of the plinian ignimbrites (explain why the presumed size of the depression of the caldera unit is generally greater than those that can be estimated on the basis of the relatively small-volume (< 10 km3 each) ignimbrites (Brousse, 1963; Brousse and Lefèvre, 1966; Mossand et al., 1982; Bourdier et al., 2016).

5.2.2. *The Aiguiller unit (2.4–1.8 Ma)*

The granitic basement underlying the Aiguiller unit is mainly affected by a series of N060E to N090E faults and fractures (Fig. 7, Gn station) that control the vent alignments in this area (Figs. 12 and 13). Some of these faults that are broadly parallel to the Saint-Sauves Fault (SSF) put in contact the granitic basement with extra-caldera ignimbrite facies of the unit and are subsequently sealed by lavas flows issued from the Banne d'Ordanche volcano (Brousse et al., 1990). This indicates a minimum age of 2.4 Ma for the youngest normal movement that acted on these faults. This is consistent with the second major phase of uplift started 5 Ma ago that is responsible for the main phase of elevation of the Mont-Dore Horst (Michon and Merle, 2001, Fig. 14).

Broadly *E*-W striking fractures are also well represented (Fig. 7, Gn station). This direction was not observed in the nearby metamorphic units. Only one site in the southeastern part of the granitic basement show similar population of fractures (Fig. 7, station GSW). The N060E to N080E faults, together with the secondary N110E orientations, appear as the main brittle structures that controlled the emplacement of the monogenetic vents (Fig. 13c). They possibly correspond to the reactivation of preexisting faults inherited from the Stephanian N-S compression (Blès et al., 1989; Bellanger et al., 2019). Therefore, E-W orientations that are only found on the northern and southern side of the Mont-Dore horst may correspond to normal faults that have controlled, together with N020E an N160E reactivated Variscan orientations, the buildup of the pyramid-shaped horst.

N-S striking faults and joints are also present in the basement of the Aiguiller unit (Fig. 7, Gn and X areas). North-South trending vertical dikes are distributed from this area to the Sancy unit, to the South (Fig. 11). This North-South distribution spatially corresponds to the N-S axis of the Mont-Dore horst. A major North-South trending fault network has been also recognized just North of the studied area (the Pontgibaud Fault Zone – PFZ; Bellanger et al., 2019). This crustal scale PFZ, parallel to the Holocene monogenetic field of the Chaîne des Puys (Boivin et al., 2017) was formed during the Visean then reactivated during the Jurassic (Bellanger et al., 2019), its most recent reactivation acting during the Oligocene-Pliocene period, contemporaneously with the uplift of the Mont-Dore horst.

The migration of the volcanism from the caldera area, located on the western side of the present-day granitic horst, to the Aiguiller massif remains largely undiscussed in the previous studies. However, this transition is contemporaneous with a change in the regional stress conditions. The NW-SE extensive regime that favored the emplacement at shallow level of a significant volume of differentiated magmas on the side of the uplifting granitic horst, progressively disappeared around 2.5 Ma, while new regional stress conditions developed with the establishment of a NW-SW compression, still active nowadays (Mazabraud et al., 2005; Fig. 14). Therefore, the final ascent of small volumes of such magmas certainly occurred under the compressional NW-SE stress field. First, although they remain limited in number, our dike measurements indicate that N-S Mesozoic fractures were the prime magma drains (Fig. 11). Second, the general E-W faults network played an important role on the location of the vents as shown by our statistical alignment analysis (Fig. 13c). Consequently, it is very likely that the intersections of these two sets of fractures were possibly the preferential locations for the volcanic vents of the Aiguiller massif as they acted as a conjugate fracture set with respect to the main NW-SE regional compressive stress.

5.2.3. *The Sancy and Massif Adventif units*

The Sancy unit is regarded as a centered volcanic complex emplaced above a small and deep magmatic reservoir in which the magmatic differentiation produced almost 75% of trachyandesites (Gourgaud, 2016; Briot et al., 1991).

Because of the lack of outcrops of the granito-gneissic basement in

the close vicinity of the Sancy unit, the potential tectonic control on the emplacement of the volcanic vents can be approached only by combining the vent alignments, and the lineament and the dike orientations analyses. All show the same primary orientations, namely N110E, N060E and N010E to N020E trends as already recognized by Lavina from dike orientations (Lavina, 1985 Fig. 11 and Fig. 13). A peculiarity comes from the Adventif unit in which the monogenetic vents, formed mainly of trachy-andesitic domes, form N020E alignments (Fig. 11).

Though the basement underlying the Sancy volcano is not exposed, the evidence suggests its brittle structures exerted a strong control on magma shallow transfer and emplacement, as the main orientations of dikes and vent alignments coincide with the regional fault directions observed in the neighborhood. In the partly eroded volcano core, the dikes cross cut mostly loose volcaniclastics. Given their high structural level and the mechanically weak properties of their surrounding deposits, it is remarkable that the Sancy dikes are well linear along their observable length and take such consistent orientations. The same observations could be made for the dikes observed in the caldera.

Why the magmatism migrated around 1.1 Ma to the South relative to the Aiguiller system, but still along the axis of the horst, remains unclear. There is no evidence of a change in the regional stress regime after the Aiguiller activity, in terms of either main stress direction or intensity. Instead, similarities in the vent alignment and dikes orientation between the Aiguiller and the Sancy units are consistent with a constant NW-SE compression over this period (Ziegler and Dèzes, 2007). In particular, the N020E and N160E Variscan fault network reactivated since the Oligocene and during the subsequent uplift remained the main active drains for the magmas, as further illustrated be the N-S trending Holocene Chaîne des Puys monogenetic field (Boivin et al., 2017).

5.3. Comparison with central volcanoes in other tectonic settings

The MDVF emplaced on an upwelling fractured granitic horst while the regional stress field evolved from a NW-SE extension to a NW-SE compression. In all units, dike orientations and vent alignments are closely related to the reactivation of properly oriented fractures in the granitic basement. This structuration can be compared to other studies of central volcanoes emplaced either in extension or compression regimes.

Considering extension settings, central volcanoes emplaced in rift zones usually show two types of dike swarms and vents distributions. Dike swarms composed mostly of inclined sheets are usually associated with vertical dike swarms parallel to the rift zone direction and along which vents align (e. g. Geitafell volcano, Burchardt and Gudmundsson, 2009; East African rift, van Wyk de Vries and van Wyk de Vries, 2018; Ardnamurchan volcanic complex, Burchardt et al., 2013). The inclined dikes forming either ring dikes or cone sheets developed in response to deflation or inflation episodes of voluminous and long-lived magma chambers (Tibaldi, 2015). In the MDVF, absence of such inclined dikes can most likely be the result of the resistant granitic fractured basement that prevented the formation of new inclined fractures. The limited vertical subsidence in the Mont-Dore caldera unit, above magma chambers of limited volume, is thus only accommodated by the reactivation of the dense preexisting fracture network.

In compressional settings, magmas tend to be transported in localized shear zones such as strike-slip or thrust faults (Gonzalez et al., 2009; van Wyk de Vries and van Wyk de Vries, 2018). Northeast of our study area only strike-slip crustal faults are recognized (SHF and SSF faults) but are too far away to have played a role in the magma ascent and storage of the MDFV. In strike slip systems, pull apart structures may collect magmas and shelters central volcanoes and calderas (van Wyk de Vries and Merle, 1998). No major strike-slip fault has been clearly identified to date in the underlying granitic basement of the Sancy volcano.

Finally, regardless of the tectonic setting, magma intrusion and the load of central volcanoes may change the local stress at shallow depth in the basement and in the volcanic edifice itself. This may lead to instabilities such as flank lateral collapses (e.g. Mt. Etna, Italy, Tibaldi and Groppelli, 2002) and gravitational deformation (e.g. Meru volcano, Tanzania, Delcamp et al., 2018). The limited size of the Sancy volcano that emplaced in a granitic basement probably prevented such events.

6. Conclusion

The Mont-Dore volcanic complex is a polygenetic volcanic field that emplaced from the mid Pliocene to the end of the Pleistocene (3.3 to 0.3 Ma) on an uplifting granito-gneissic basement. During this period the regional stress field evolved around 2.5 Ma from a NW-SE extension to a NW-SE compression, the later stress field being still active nowadays.

We analyzed faults kinematics, orientations of fractures and regional lineaments in the Variscan basement and we measured strikes of dikes and volcanic centers alignments. We evidenced the influence of the brittle structuration of the underlying basement on the ascent at shallow depth and final emplacement of magmas by reactivation of properly oriented preexisting late Variscan and Mesozoic faults networks with respect to the stress field. The late-Variscan N020E, and secondary N160E, crustal faults were reactivated since the Oligocene and mostly channeled at depth the magmas. In addition, similarly oriented crustal faults controlled both the final storage of differentiated magmas in the shallow crust and the spatial distribution of the vents in the Aiguiller unit and emplacement of the Sancy unit. Finally, we evidenced N020E, flat-lying, shear fractures relevant to the Miocene NW-SE compressional regional stress field, but whose influence on magmas emplacement was negligible. The main exception arises before 2.5 Ma when N060E and N135E faults controlled the emplacement of the caldera unit in an NW-SE extensional context. This further possibly favored the storage at shallow depth of a large volume of magma that led to the preeruptive differentiation of the ignimbritic products (Briot et al., 1991) and the collapse of a large depression.

This study highlights the close relationships between reactivated Variscan to Mesozoic brittle structures of the underlying basement and the transfer, the storage and the final emplacement of the Mont-dore volcanics as also established for monogenetic, mostly basaltic, volcanic fields such as the Holocene Chaîne des Puys to the North (Le Corvec et al., 2013; Boivin et al., 2017).

CRediT authorship contribution statement

Camille Daffos: Conceptualization, Formal analysis, Writing – original draft, Writing – review & editing. **Laurent Arbaret:** Conceptualization, Data curation, Funding acquisition, Project administration, Writing – original draft, Writing – review & editing. **Jean-Louis Bourdier:** Conceptualization, Formal analysis, Writing – original draft, Writing – review & editing. **Charles Gumiaux:** Conceptualization, Formal analysis, Writing – original draft, Writing – review & editing.

Declaration of competing interest

The authors declare the following financial interests/personal relationships which may be considered as potential competing interests.

Arbaret Laurent reports financial support was provided by French Agency for Research (Agence Nationale de la Recherche, ANR).

Data availability

Data will be made available on request.

Acknowledgments

This work was financed by TLS GEOTHERMICS (Contract CNRS N° 30040422). CD and LA are supported by the French Agency for Research

(Agence Nationale de la Recherche, ANR) through the grant MECA-MUSH ANR-19-0315CE-0007. Abdelsalam Elshaafi and an anonymous reviewer are thanked for helpful comments.

References

Acocella, V., 2021. Volcano-Tectonic Processes, vol. 567. Springer, Switzerland.

Allmendinger, R.W., Cardozo, N.C., Fisher, D., 2012. Structural Geology Algorithms: Vectors & Tensors: Cambridge. Cambridge University Press, England, p. 289.

Babuška, V., Plomerová, J., Vecsey, L., Granet, M., Achauer, U., 2002. Seismic anisotropy of the French Massif Central and predisposition of Cenozoic rifting and volcanism by Variscan suture hidden in the mantle lithosphere. Tectonics 21, 11-1 – 11-20.

Baize, S., Cushing, E.M., Lemeille, F., Jomard, H., 2013. Updated seismotectonic zoning scheme of metropolitan France, with reference to geologic seismotectonic data. Bull. Soc. Géol. de France 184, 225–259.

Baubron, J.C., Cantagrel, J.M., 1980. Les deux volcans des Monts-Dore (Massif Central français). Comptes-Rendus de l'Acad. des Sci. Paris, sér D 290, 1409–1412.

Beggan, C., Hamilton, C.W., 2010. New image processing software for analyzing object size-frequency distribution, geometry, orientation and spatial distribution. Comput. Geosci. 36, 539–549.

Bellanger, M., Hermant, B., Galibert, S., Auxièrte, J.-L., 2019. Fault-Controlled Hydrothermal System Associated with Major Crustal Fault Zone: Future Drilling Target to Asses the Deep Geothermal Potential – The Sioule License Project. European Geotherrmal Congress, Den Haag, The Netherlands.

Bergerat, F., Mugnier, J.-L., Guellec, S., Trufferrt, C., Cazes, M., Damotte, B., Roure, F., 1990. Extensional tectonics and subsidence of the Bresse Basin: an interpretation from ECORS data. Mém. Soc. Géol. Fr. 156, 145–156.

Blès, J.L., Bonijoly, D., Castaing, C., Gros, Y., 1989. Successive post-Variscan stress fields in the French Massif Central and its borders (Western European plate): comparison with geodynamic data. Tectophysics 169, 79–111.

Boivin, P., Besson, J.C., Briot, D., Deniel, C., Gourgaud, A., Labazuy, P., Langlois, E., de Larouzière, F.D., Livet, M., Merciecca, C., Médard, E., Mergoil, J., Miallier, D., Morel, J.M., Thouret, J.C., Vernet, G., 2017. Volcanologie de la Chaîne des Puys Massif Central Français. 6e édition, bilingue. In: Édition Parc Naturel Régional des Volcans d'Auvergne Château de Montlosier, Randanne, 63970 Aydat, p. 200. Carte 1/25 000, 120x90 cm.

Bourdier, J.L., Auxerre, M., Arbaret, L., Pichavant, M., 2016. Composition and correlation criteria of rhyolitic ignimbrites in the Monts Dore volcanic field (France). Bull. Soc. Géol. France 187-6, 261–273.

Breitkreuz, C., Rocchi, S., 2018. Physical Geology of Shallow Magmatic Systems - Dykes, Sills and Laccoliths. Advances in Volcanology. Springer.

Briot, D., Cantagrel, J.M., Dupuy, C., Harmon, R.S., 1991. Geochemical evolution in crustal magma reservoirs: Trace-element and Sr-Nd-O isotopic variations in two continental intraplate series at Monts Dore, Massif Central, France. Chem. Geol. 89, 281–303.

Brousse, R., 1961. Minéralisation et pétrographie des roches volcaniques du Massif du Mont-Dore. Bull. Soc. Fr. Minéral. Cristallogr. 84-2, 131–186.

Brousse, R., 1963. 1963. Identification de deux coulées de ponces dans le massif volcanique du Mont-Dore. Compte-rendu de l'Acad. des Sci. Paris D-257, 2869–2871.

Brousse, R., 1971. Magmatologie du volcanisme néogène et quaternaire du Massif Central. In: Symposium Géologie, géomorphologie et structure profonde du Massif Central français, Clermont-Ferrand. Plein Air Service Ed, pp. 377–478.

Brousse, R., Lefèvre, C., 1966. Nappes de ponces du Cantal et du Mont-Dore ? Leurs aspects volcanologiques, pétrographiques et minéralogiques. Bull. Soc. Géol. France 7-8, 223–245.

Brousse, R., Tempier, P., 1981. Carte géol. France (1/50 000), feuille BOURG-LASTIC (716) - Orléans : Bureau de recherches géologiques et minières. Notice explicative par Brousse R., Tempier P., Rançon J.P., Veyret-Mekdjian Y. et coll. (1989), p. 78.

Brousse, P., Suire, J., Tempier, P., Le Garrec, M.J., Veyre-Mekdjian, Y., Medhizadeh, H., Mervoyer, B., Musengié, M., 1990. Carte géol. France (1/50 000), feuille La Tour-d'Auvergne (740) — Orléans : Bureau de recherches géologiques et minières. Notice explicative par Brousse P., Rançon J.P., Le Garrec M. J., Tempier P., Suire J., Veyret-Mekdjian Y., D'Arcy D., Perichaud J.J. (1990), p. 68.

Brun, A., 1975. La fosse d'effondrement volcano-tectonique de la Bourboule Le Mont-Dore et ses bordures. Bull. de l'Assoc. Française Pour l'étude du Quaternaire. 11-1, 25–43. https://doi.org/10.3406/quate.1974.1237.

Burchardt, S., Gudmundsson, A., 2009. The infrastructure of Geitafell Volcano, Southeast Iceland. In: Thordarson, T., Self, S., Larsen, G., Rowland, S., Hoskuldsson, A. (Eds.), Studies in Volcanology: The Legacy of George Walker. Special Publications of IAVCEI 2. Geological Society, London, pp. 349–370.

Burchardt, S., Troll, V.R., Mathieu, L., Emeleus, H.C., Donaldson, C.H., 2013. Ardnamurchan 3D cone-sheet architecture explained by a single elongate magma chamber. Sci. Rep. 3, 2891. https://doi.org/10.1038/srep02891.

Bursik, M., 2009. A general model for tectonic control of magmatism: examples from Long Valley Caldera (USA) and El Chichón (México). Geofis. Int. 48 (1) https://doi.org/10.22201/igeof.00167169p.2009.48.1.106.

Cantagrel, J.M., Baubron, J.C., 1983. Chronologie K-Ar des éruptions dans le massif volcanique des Mont-Dore : implications volcanologiques. Géol. Fr. (2), I, 1-2, 123–142.

Cantagrel, J.M., Briot, D., 1990. Avalanches et coulées de débris : le volcan du Guéry – Où est la caldera d'effondrement dans le massif des Monts-Dore ? Compte rendu de l'Acad. des Sci. Paris II-311, 219–225.

Carlino, S., Tramelli, A., Somma, R., 2014. Caldera subsidence in extensional settings. Bull. Volcanol. 76, 870.

Cebrià, J.M., Martin-Escorza, C., Lopez-Ruiz, J., Moran-Zenteno, D.J., Martiny, B.M., 2011. Numerical recognition of alignments in monogenetic volcanic areas: Exemples from the Michoacan-Guanajuato Volcanic Field in Mexico and Calatrava in Spain. J. Volcanol. Geotherm. Res. 201, 73–82.

Cembrano, J., Lara, L., 2009. The link between volcanism and tectonics in the southern volcanic zone of the Chilean Andes: a review. Tectonophysics 471, 96–113.

Cembrano, J., Moreno, H., 1994. Geometría y naturaleza contrastante del volcanismo cuaternario entre los 38°S y 46°S: ¿Dominios compresionales y tensionales en un régimen transcurrente? Congreso Geoló. Chileno No. 7 Actas 1, 240–244.

Clark, P.J., Evans, F.C., 1954. Distance to nearest neighbor as a measure of spatial relationships in populations. Ecology 35, 445–453.

Connor, C.B., 1990. Cinder cone clustering in the TransMexican Volcanic Belt: implications for structural and petrologic models. J. Geophys. Res. 95, 19,395–19,405.

Connor, C.B., Condit, C.D., Crumpler, L.S., Aubele, J.C., 1992. Evidence of Regional Structural Controls on Vent distribution – Springerville Volcanic Field, Arizona. J. Geophys. Res.-Solid Earth 97, 12349–12359.

Delcamp, A., Poppe, S., Detienne, M., Paguican, E.M.R., 2018. Destroying a volcanic edifice-interactions between edifice instabilities and the volcanic plumbing system. In: Volcan. Igneous Plumb, Syst. Underst. Magma Transp. Storage, Evol. Earth's Crust, pp. 231–257.

Dèzes, P., Schmid, S.M., Ziegler, P.A., 2004. Evolution of the Cenozoic Rift System: interaction of the Alpine and Pyrenean orogens with their foreland lithosphere. Tectonophysics 389, 1–33.

Elshaafi, A., Gudmundsson, A., 2016. Volcano-tectonics of the Al Haruj Volcanic Province, Central Lybia. J. Volcanol. Geotherm. Res. 325, 189–202.

Faure, M., 1995. Late orogenic carboniferous extensions in the Variscan French Massif Central. Tectonics 14-1, 132–153.

Feybesse, J.L., Lespinasse, M., 1987. Contrôle structural des circulations hydrothermales du Cézallier. Bull. Soc. Geol. France 4, 63–80.

Gonzalez, G., Cembrano, J., Aron, F., Veloso, E.E., Shyu, J.B.H., 2009. Coeval compressional deformation and volcanism in the Central Andes, case studies from northern Chile (23°S – 24°S). Tectonics 28, TC6003. https://doi.org/10.1029/2009TC002538.

Gourgaud, A., 2016. Volcanism of the Monts Dore (French Massif Central). In: Sime-Ngando, T., Boivin, P., Chaperon, E., Jézéquel, D., Meybeck, M. (Eds.), Lake Pavin. Springer International Publishing, Switzerland, pp. 83–89.

Gudmundsson, A., 2006. How local stresses control magma-chamber ruptures, dyke injections, and eruptions in composite volcanoes. Earth Sci. Rev. 79 (1–2), 1–31.

Gudmundsson, A., 2011. Rock Fractures in Geological Processes. Cambridge University Press.

Gudmundsson, A., 2020. Volcanotectonics. Understanding the Structure, Deformation and Dynamics of Volcanoes. Cambridge University Press.

Gudmundsson, A., Brenner, S.L., 2005. On the conditions of sheet injections and eruptions in stratovolcanoes. Bull. Volcanol. 67, 768–782.

Heidbach, O., Rajabi, M., Reiter, K., Ziegler, M., WSM Team, 2016. World Stress Map Database Release 2016. GFZ Data Services. https://doi.org/10.5880/WSM.2016.001.

IGN, 2011. Institut National de l'Information Géographique et Forestière, France. Geoservices IGN, *BD ALTI 25m v2.0,* from. https://geoservices.ign.fr/bdalti.

Joly, A., Chen, Y., Faure, M., Martelet, G., 2007. A multidisciplinary study of a syntectonic pluton close to a major lithospheric-scale fault. Relationships between the Montmarault granitic massif and the Sillon Houiller Fault in the Variscan French Massif Central: 1. Geochronology, mineral fabrics, and tectonic implications. J. Geophys. Res. 112 (10).

Kavanagh, J.L., 2018. Mechanisms of Magma Transport in the Upper Crust-Dyking, Volcanic and Igneous Plumbing Systems: Understanding Magma Transport, Storage, and Evolution in the Earth's Crust. Elsevier Inc. https://doi.org/10.1016/B978-0-12-809749-6.00003-0

Kavanagh, J.L., Burns, A.J., Hazim, S.H., Wood, E.P., Martin, S.A., Hignett, S., Dennis, D. J., 2018. Challenging dyke ascent models using novel laboratory experiments: Implications for reinterpreting evidence of magma ascent and volcanism. J. Volcanol. Geotherm. Res. 354, 87–101.

Lavina, P., 1985. Le volcan du Sancy et le « Massif Adventif » (Massif des Monts Dore; Massif Central Français). Ph.D. thesis,. Université de Clermont-Ferrand, p. 210.

Le Corvec, N., Bernhard Spörli, K., Rowland, J., Lindsay, J., 2013. Spatial distribution and alignments of volcanic centers: Clues to the formation of monogenetic volcanic fields. Earth Sci. Rev. 124, 96–114.

Lustrino, M., Wilson, M., 2007. The circum-Mediterranean anorogenic Cenozoic igneous province. Earth Sci. Rev. 81, 1–65.

Maccaferri, F., Bonafede, M., Rivalta, E., 2011. A quantitative study of the mechanisms governing dike propagation, dike arrest and sill formation. J. Volcanol. Geotherm. Res. 208 (1–2), 39–50.

Marrett, R.A., Allmendinger, R.W., 1990. Kinematic analysis of fault-slip data. J. Struct. Geol. 12, 973–986.

Martí, J., López, C., Bartolini, S., Becerril, L., Geyer, A., 2016. Stress Controls of Monogenetic Volcanism: a Review. Front. Earth Sci. 4, 106. https://doi.org/10.3389/feart.2016.00106.

Mazabraud, Y., Béthoux, N., Deroussi, S., 2005. Characterisation of the seismological pattern in a slowly deforming intraplate region: Central and western France. Tectonophysics 409, 175–192.

Menand, T., 2011. Physical controls and depth of emplacement of igneous bodies: a review. Tectonophysics 500, 11–19.

Ménard, J.-J., Clocchiatti, R., Maury, R.C., Brousse, R., 1980. Origine des ponces rhyolitiques du Mont-Dore (Massif central, France): Arguments pétrologiques. C. R. Acad. Sci. Paris Ser. D 290, 559–562.
Merle, O., Michon, L., 2001. The formation of the west European rift: a new model as exemplified by the Massif Central area. Bull. Soc. Géol. France 172-2, 213–221.
Merle, O., Aumar, C., Labazuy, P., Merciecca, C., Buvat, S., 2023. Structuration tertiaire et quaternaire du plateau des Dômes (Chaîne des Puys, Massif central, France). Géol. Fr. 3, 1–22.
Michon, L., Merle, O., 2001. The evolution of the Massif Central rift: spatio-temporal distribution of the volcanism. Bull. Soc. Géol. France 172-2, 201–211.
Morel, J.M., 1987. Volcanologie du massif de l'Aiguiller (Monts Dore, Massif Central Français): Etude pétrographique, dynamique, structural et rhéologie des coulées de boue associées. Ph.D. thesis,. Université de Clermont-Ferrand, p. 200.
Mossand, Ph., Cantagruel, J.M., Vincent, P.M., 1982. La caldera de Haute-Dordogne. Age et limites (Massif des Mont-Dore, France). Bull. Soc. Géol. France 7-24, 727–738.
Nomade, S., Scaillet, S., Pastre, J.F., Nehlig, P., 2012. Pyroclastic chronology of the Sancy stratovolcan (Mont-Dore, French Massif Central): New high-precision 40Ar/39Ar constraints. J. Volcanol. Geotherm. Res. 225-226, 1–12.
Pastre, J.F., Cantagrel, J.M., 2001. The Mont Dore tephrostratigraphy (Massif Central, France). Quaternaire 12-4, 249–267.
Petford, N., 2000. Granite magma formation, transport and emplacement in the Earth's crust. Nature 408 (6813), 669–673.
Pollard, D.D., 1987. Theoretical displacements and stresses near fractures in rock: with applications to faults, joints, veins, dikes, and solution surfaces. Fract. Mech. Rock 277–349.
QGIS.org, 2024. QGIS Geographic Information System. QGIS Association. http://www.qgis.org.
Rubin, A.M., 1995. Propagation of magma filled cracks. Annu. Rev. Earth Planet. Sci. 23p, 287–336. https://doi.org/10.1146/annurev.ea.23.050195.001443.
Thiery, V., Rolin, P., Marquer, D., Cocherie, A. Mark, Fanning, C., Rossi, P., Marquer, D., A., C., and others, 2009. Visean sinistral wrench faulting along the Sillon Houiller in the French Massif Central : late Variscan tectonic implications. Bull. Soc. Géol. de France 180, 513–528.
Tibaldi, A., 2015. Structure of volcano plumbing systems: a review of multi-parametric effects. J. Volcanol. Geotherm. Res. 298, 85–135.
Tibaldi, A., Groppelli, G., 2002. Volcano-tectonic activity along structures of the unstable NE flank of Mt. Etna (Italy) and their possible origin. J. Volcanol. Geotherm. Res. 11, 277–302.
van Wyk de Vries, B., Merle, O., 1998. Extension induced by volcanic loading in regional strike-slip zones. Geology 26, 983–986.
van Wyk de Vries, B., van Wyk de Vries, M., 2018. Tectonics and volcanic and igneous plumbing systems. In: Burchardt, S. (Ed.), Volcanic and Igneous Plumbing Systems. Elsevier, pp. 167–189.
Vanderhaeghe, O., Laurent, O., Gardien, V., Moyen, J.-F., Gébelin, A., Chelle-Michou, C., Courinié, S., Villaros, A., Bellanger, M., 2020. Flow of partially molten crust controlling construction, growth and collapse of the Variscan orogenic belt: the geologic record of the French Massif Central. BSGF Earth Sci. Bullet. 191, 25.
Varet, J., Stieltjes, L., Gerard, A., Fouillac, C., 1980. Prospection géothermique intégrée dans le massif du Mont-Dore. Adv. European Geotherm. Res., Strasbourg 1980, 154–201.
Vincent, P.M., 1980. Volcanisme et chambres magmatiques : l'exemple des Monts-Dore. Mém. hors-série de la Soc. Géol. de France 10, 71–85.
Von Veh, M.W., Németh, K., 2009. An Assessment of the alignments of vents based on geostatistical analysis in the Auckland Volcanic Field, New Zealand. Géomorphologie 2009 (15–3), 175–186.
Wadge, G., Cross, A.M., 1988. Quantitative methods for detecting aligned points: an application to the volcanic vents of the Michoan-Guanajuato volcanic field, Mexico. Geology 16 (9), 815–818.
Westaway, R., 2004. Pliocene and Quaternary surface uplift evidenced by sediments of the Loir-Allier river system (France). Quaternary 15, 103–115.
Ziegler, P.A., Dèzes, P., 2007. Cenozoic uplift of Variscan Massifs in the Alpine foreland: timing and controlling mechanisms. Glob. Planet. Chang. 58, 237–269.